



Marine Renewables Infrastructure Network

WP4: Research to innovate and improve infrastructures, technologies and techniques

Non-intrusive wave field measurement

Authors:

Sylvain Bourdier	ECN
Keith Dampney	EMEC
Hernan Fernandez	LUH
Guiomar Lopez	PU
Jean-Baptiste Richon	UEDIN



Status: Final
Revision: 4
Date: 10-Nov-2014



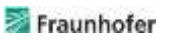
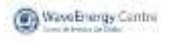
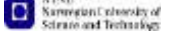
ABOUT MARINET

MARINET (Marine Renewables Infrastructure Network for Emerging Energy Technologies) is an EC-funded consortium of 29 partners bringing together a network of 42 specialist marine renewable energy testing facilities. MARINET offers periods of free access to these facilities at no cost to research groups and companies. The network also conducts coordinated research to improve testing capabilities, implements common testing standards and provides training and networking opportunities in order to enhance expertise in the industry. The aim of the MARINET initiative is to accelerate the development of marine renewable energy technology.

Companies and research groups who are interested in availing of access to test facilities free of charge can avail of a range of infrastructures to test devices at any scale in areas such as wave energy, tidal energy and offshore-wind energy or to conduct specific tests on cross-cutting areas such as power take-off systems, grid integration, moorings and environmental data. In total, over 700 weeks of access is available to an estimated 300 projects and 800 external users.

MARINET is consists of five main areas of focus or 'Work Packages': Management & Administration, Standardisation & Best Practice, Transnational Access & Networking, Research and Training & Dissemination. The initiative runs for four years until 2015.

Partners

  	<p>Ireland University College Cork, HMRC (UCC_HMRC) <i>Coordinator</i> Sustainable Energy Authority of Ireland (SEAI_OEDU)</p>	<p>Netherlands Stichting Tidal Testing Centre (TTC) Stichting Energieonderzoek Centrum Nederland (ECNeth)</p>	 
	<p>Denmark Aalborg Universitet (AAU) Danmarks Tekniske Universitet (RISOE)</p>	<p>Germany Fraunhofer-Gesellschaft Zur Foerderung Der Angewandten Forschung E.V (Fh_IWES) Gottfried Wilhelm Leibniz Universität Hannover (LUH) Universitaet Stuttgart (USTUTT)</p>	  
	<p>France Ecole Centrale de Nantes (ECN) Institut Français de Recherche Pour l'Exploitation de la Mer (IFREMER)</p>	<p>Portugal Wave Energy Centre – Centro de Energia das Ondas (WavEC)</p>	
      	<p>United Kingdom National Renewable Energy Centre Ltd. (NAREC) The University of Exeter (UNEXE) European Marine Energy Centre Ltd. (EMEC) University of Strathclyde (UNI_STRATH) The University of Edinburgh (UEDIN) Queen's University Belfast (QUB) Plymouth University (PU)</p>	<p>Italy Università degli Studi di Firenze (UNIFI-CRIACIV) Università degli Studi di Firenze (UNIFI-PIN) Università degli Studi della Tuscia (UNI_TUS) Consiglio Nazionale delle Ricerche (CNR-INSEAN)</p>	   
 	<p>Spain Ente Vasco de la Energía (EVE) Tecnalia Research & Innovation Foundation (TECNALIA)</p>	<p>Norway Sintef Energi AS (SINTEF) Norges Teknisk-Naturvitenskapelige Universitet (NTNU)</p>	 
	<p>Belgium 1-Tech (1_TECH)</p>		

DOCUMENT INFORMATION

Title	Non-intrusive wave field measurement
Distribution	Consortium partners and EC
Document Reference	MARINET Deliverable D4.05

REVISION HISTORY

Rev.	Date	Description	Prepared by (Name & Org.)	Approved By (Task Leader)	Status (Draft/Final)
01	31/07/2014	First draft	Sylvain Bourdier ECN		Draft
02	08/09/2014	Advanced draft	Sylvain Bourdier ECN		Draft
03	17/09/2014	Draft including corrections from Jochen Giebhart	Sylvain Bourdier ECN		Draft
04	10/11/2014	Approved by TL/WPL	J. Giebhardt	yes	Final

ACKNOWLEDGEMENT

The work described in this publication has received funding from the European Union Seventh Framework Programme (FP7) through the Infrastructures initiative under grant agreement no. 262552, MARINET.

LEGAL DISCLAIMER

The views expressed, and responsibility for the content of this publication, lie solely with the authors. The European Commission is not liable for any use that may be made of the information contained herein. This work may rely on data from sources external to the MARINET project Consortium. Members of the Consortium do not accept liability for loss or damage suffered by any third party as a result of errors or inaccuracies in such data. The information in this document is provided “as is” and no guarantee or warranty is given that the information is fit for any particular purpose. The user thereof uses the information at its sole risk and neither the European Commission nor any member of the MARINET Consortium is liable for any use that may be made of the information.

EXECUTIVE SUMMARY

The measurement of the wave climate plays a vital role in many stages of the development of Marine Renewable Energy (MRE). Wave climate measurements are for example needed for resource characterisation for identification of potential sites for commercial developments or for environmental monitoring of MRE sites. Wave measurement is also needed in the development of MRE converters, during testing phases at model scale in a controlled environment up to testing phases at full scale out at sea.

Non-intrusive instrumentation can provide several benefits compared to in-situ instruments. The fact that the instrumentation does not interfere with the wave field to be measured can be an advantage in laboratory experiments where it reduces unwanted disturbances, but also at sea where the instrument does not (or less) suffer from exposure to sea water corrosion, bio-fouling, wave load and damages from human activities.

The Marinet program dedicated a work package (WP4- Research to innovate and improve Infrastructures, technologies and techniques) to improve the facilities, operational techniques and instrumentation at European Infrastructures for Offshore Renewable Energy Research. Within this work package, a task (T4.1.2) was identified to develop innovative non-intrusive methods in order to characterize the water wave conditions, for model scale measurements and full scale. Its aim was to build operational instruments and to produce guidelines about their use in WEC studies.

This document presents and discusses some recent developments in a number of non-intrusive techniques for the measurement of water waves, with particular attention paid to the recent works done by some partner institutions of the Marinet program. Because the spatial and temporal scales required for the study of water wave dynamics are different out at sea from those needed at model scale, the techniques developed do differ. Late developments in non-intrusive techniques for ocean wave field measurement at sea are presented in a first section, while those concerning techniques used in laboratories are presented in a second section.

CONTENTS

1	INTRODUCTION	6
2	NON-INTRUSIVE WAVE FIELD MEASUREMENT AT SEA	9
2.1	ACOUSTIC SENSORS	9
2.1.1	ADCPs	9
2.1.2	Ultrasonic sensors	11
2.2	RADAR REMOTE SENSING	11
2.2.1	Radar altimeters.....	12
2.2.2	Synthetic Aperture Radars (SAR).....	13
2.2.3	Marine radars.....	15
2.2.4	HF radar.....	21
2.3	IMAGING METHODS	27
2.3.1	Stereo-photogrammetry	27
2.4	LIDARS.....	30
3	NON-INTRUSIVE WAVE FIELD MEASUREMENT IN WAVE TANKS	33
3.1	OPTICAL SENSORS.....	33
3.1.1	Optical triangulation wave probe	34
3.1.2	Laser slope gauges	37
3.1.3	Lidars	38
3.2	ACOUSTIC SENSORS.....	38
3.2.1	Ultrasonic sensors	38
3.3	RADARS.....	39
3.4	IMAGING METHODS	39
3.4.1	Laser sheet-based technique for free surface measurement	40
3.4.2	Particle Image velocimetry.....	41
3.4.3	Stereo-Imaging.....	42
3.5	COMBINED LASER-SCANNER AND VIDEO HYBRID SYSTEM	43
3.5.1	Introduction.....	43
3.5.2	Materials and methods	43
3.5.3	Results and discussion	46
4	CONCLUSIONS	49
5	REFERENCES	51

1 INTRODUCTION

The ability to measure the characteristics of water waves is essential to the development of Marine Renewable Energies (MRE), and particularly to the development of Wave Energy Converters (WEC). Four main drivers were for example identified by the authors of the Equimar D2.2 (Venugopal, et al., 2011) for the measurement of the wave, tide and (possibly) wind climate:

- **Characterisation of the Energy Resource:**

For the purpose of MRE, a primary focus is to ascertain the level of resource, at an appropriate level of confidence, through the development of a project. This information provide the basis for a specification of power (in time) and the energy to be produced over the length of the project. It is necessary to investors, utilities and government (both national and local).

- **Engineering Design:**

Although the major design considerations for any device will be decided, it is probable that individual sites may require adaptation of the base design. Certainly, issues of wave and current loading will have to be considered on a site-by-site basis for the design of the moorings. This information will be necessary to designers, constructors, insurers and classification societies.

- **Conduct of Marine Operations:**

For a fully operating project, the assessment and prediction of the wave, wind and tidal characteristics are necessary to predict the installation & maintenance strategies. This information will be necessary to designers, constructors, marine contractors, insurers and classification societies.

- **Calibration and validation of numerical models:**

In complex sites, the use and accuracy of any model produced will benefit from “calibration” with measured data.

They stated that marine energy resource assessments may be conducted to various levels of detail depending on the stage of a project. Wave climate may be first roughly assessed, and predicted, to identify suitable geographic locations for deployment. Once suitable areas have been identified, detailed assessments will be necessary to characterise specific sites.

It can be added that the assessment of the environmental impacts of MRE is also a key point in their development, for example to obtain authorisations from the regulatory bodies. Measurement of environmental conditions, including of the wave climate, over extended periods of time, is necessary to the thorough assessment of environmental impacts.

The first phases of development of a marine energy converter are more concerned with validating the concept of the device using numerical simulation and tank testing of small scale models (Technology Readiness Levels TRL 1-3). At TRL 4, the engineering design of a full-scale prototype should be drawn up using estimates of loads in extreme conditions, obtained from tank testing of scale models at intermediate scales. Physical modelling of a device is therefore a key step in the first phases of its development. Very good knowledge of the wave climate simulated at model scale is one of the key inputs necessary to the analysis of the response of a model's device. Accurate measurement of the waves generated at model scale in a basin is an essential skill in coastal laboratories.

Instrumentation and techniques for water wave measurement have been developed since a long time both for the real environment at sea and in laboratories. Given the similarity of the physical

processes studied, one could think that instrumentation used for measuring waves at sea and in laboratories could be similar.

These two environments are however very different in some aspects, implying different types of constraints for the sensors used in each environment. Underwater vision, for example, can be very poor at sea due to water turbidity, while transparent water in wave tanks allows good vision and the recording of a body's motion with cameras, for example using underwater trajectography. On the contrary, water turbidity is beneficial when using stereo-vision systems to measure water waves at sea, as are cloudy lighting conditions. Stereo-vision is more difficult to implement in wave tanks with clear water and directional lights. Water salinity and marine growth can be difficult to deal with when using sensors at sea. Environmental constraints at sea also include the presence of marine fauna and flora. The emission of sound waves in the ocean, e.g. as generated by active sonars, is known to be affecting marine mammals, which rely on sound for a wide range of biological functions, including communication, navigation, foraging, and predator detection.

As a result, instrumentation used at sea or in wave tanks to measure water waves can be very different.

A wide range of systems for ocean wave measurement exists. The choice of one is usually made considering depth, access, wave conditions, or the required level of details required in the data.

In-situ instruments are those located at the water surface (like a floating buoy), below the water surface (like a pressure probe or an acoustic sensor placed at the sea bottom), or surface-piercing (like a resistive wave gauge). Offshore, the most commonly used in-situ instruments are wave buoys, and recently directional wave buoys, equipped with Global Positioning System (GPS). They return time series of sea surface elevation from which wave height, period and direction can be derived by spectral or direct analysis of the time series. Near-shore, submerged pressure sensors arrays, acoustic probes, wave staffs and current meters are commonly used. In-situ measurements provide realistic data but they are not widely available, because they are expensive and difficult to obtain in the harsh marine environment.

In a strict sense, in-situ instruments are considered intrusive, as they penetrate the water agitated by waves and currents.

Some in-situ instruments can be placed far enough from their measurement volume to not disturb (or only minimally) the wave field they measure. That is for example the case for bottom-mounted instruments placed further down than a wavelength below the free surface. In this case, as they do not interfere with the physical processes to be measured, they can be considered as only lightly intrusive. One of the main limitations of such in-situ non-intrusive systems is their exposition to the harsh marine environment.

Remote-sensing instruments, placed above the water on a fixed (e.g. a tower at sea) or moving platform (e.g. a ship, an airplane or a satellite), are the only ones that can be truly considered as non-intrusive. The principle of most of the remote-sensing techniques is to receive reflections of the sea surface of visible or infra-red light or radar energy (Holthuijsen, 2007). They are generally not sensitive to the marine environment but they may be sensitive to atmospheric conditions (rain, clouds, water vapour contained in fog). Remote-sensing instruments can also allow covering large measurement volumes in short periods of time. This is for example the case for radar measurements of ocean waves, particularly if the platform is an aircraft or a satellite and for stereo-vision of water waves at sea or in wave tanks. Out at sea, one of their main advantages is also that the instrument is not or less subject to the marine environment, implying less exposure to sea water corrosion, bio-fouling and wave loads.

In laboratory experiments, traditional instrumentation for wave measurement include resistance type gauges and capacitance wire gauge, the latter being best suited to the measurement of large waves. Arrays of a number of such gauges are usually used to measure the directional spectra of the waves in a wave tank. They are cheap and robust and their calibration is simple but needs to be done

regularly. They are intrusive, which can be a problem when measuring very small waves (due to radiated waves), and very large waves (due to wave loading). They can also for example generate non-negligible waves in a towing tank when towed at high speed.

An advantage of point-measurement with non-intrusive instrumentation is then that the instrument does not interfere with the wave field to be measured. Unwanted disturbances are also removed. Instruments and techniques for remote-sensing of water waves can allow a larger measurement area, like a two-dimensional measurement of the water surface, as when using a laser sheet or a lidar, or a three-dimensional measurement of the free surface, as when using stereo-photogrammetry.

The Marinet program dedicated a work package (WP4- Research to innovate and improve Infrastructures, technologies and techniques) to improve the facilities, operational techniques and instrumentation at European Infrastructures for Offshore Renewable Energy Research. Within this work package, a task (T4.1.2) was identified to develop innovative non-intrusive methods in order to characterize the water wave conditions, for model scale measurements and full scale. Its aim was to build operational instruments and to produce guidelines about their use in WEC studies.

In this report, some of the late developments in non-intrusive techniques for wave field measurement at sea are reported in a first section, while those concerning techniques used in laboratories are presented in a second section. Particularly attention, and space, is given to the works done recently in four different institutions taking part in the Marinet program. Two contributions were made concerning remote sensing of ocean waves. One, presented in section 2.2.3, on the comparison of measurements made at the European Marine Energy Centre (EMEC) with marine radars to in-situ measurements made with buoys and ADCPs, the other presented in section 2.2.4 on the comparison of HF radar measurements around the Wave Hub test site area with in-situ measurements and their use for the calibration of a numerical model of the area. Two other contributions describe non-intrusive wave field measurement techniques in wave tanks: the first one presented in section 3.1.1 reports developments of an optical wave probe, the second one presented in section 3.5 reports on a system combining laser scanner measurements and video, for wave measurement in the swash zone.

2 NON-INTRUSIVE WAVE FIELD MEASUREMENT AT SEA

The first global source of ocean wave data is visual observations carried out for meteorological purposes on board of commercial ships, which started to be archived by 1850 e.g. by British Meteorological Office. Their accuracy is considered good for direction, acceptable for wave height and of lower quality for period (IEA-OES, 2009). Nowadays, the World Meteorological Organization (WMO) Voluntary Observing Ships (VOS) scheme still runs, even if the number of VOS decreased to about four thousands (http://www.vos.noaa.gov/vos_scheme.shtml). The ships are equipped with different types of on-board instrumentation and provide ground truth for validation of remote sensed measurements, e.g. by satellites.

Classical methods for wave measurement include arrays of sensors like capacitance wire gauges or bottom-mounted pressure sensors. However these are usually complex to install. Pitch-and-roll buoys are also widely used but they are expensive, prone to damage and vandalism, and have mooring issues in shallow coastal waters (Birch, Fissel, Borg, Lee, & English, 2004). Bottom mounted pressure-velocity (PUV) sensors are less expensive but are limited in effective working depths to less than 10-15 *m* due to the high degree of attenuation in the high frequency portion of the wave signal of pressure and velocity.

Many instruments and analysis techniques have been developed both for in-situ and remote measurement of ocean gravity waves. The emphasis is put nowadays on measuring the directional spectra of ocean waves. A large number of instruments, using different operating principles or technologies, are now available.

Classical methods have been complemented by new technologies such as the displacement and GPS buoy, acoustic Doppler profilers, marine X-band radars, coastal HF radars and real or synthetic aperture radars. Lately, advances in stereo vision analysis allowed very accurate measurements of three-dimensional wave fields. Lidars have also been used with some success for wave field measurement, both at sea and in laboratories.

2.1 ACOUSTIC SENSORS

2.1.1 ADCPs

Acoustic Doppler Current Profilers (ADCPs) have become widely used in offshore engineering for multiple goals, particularly since their adaptation to the measurement of directional wave spectra. They are used in the development of MRE at different stages, from initial resource assessments to wave and tidal measurements during testing phases. They can be considered non-intrusive because they are deployed from their measurement volumes and usually do not affect the physical processes to be measured.

ADCPs are acoustic current meters measuring the water velocities over a depth range using the Doppler effect of sound waves (of frequency ranging between 38 *KHz* to some *MHz*) scattered back by the particles within the measurement volume. They return average velocity values over adjustable-length cells along the acoustic beams. They can estimate the directional properties of the wave field through the use of multiple acoustic beams, or by combination of acoustic measurement with a pressure or surface tracking measurement.

Most commonly used ADCPs are made by Teledyne, Sontek or Nortek. Two ADCPs made for wave field measurement are briefly presented here, to illustrate the differences in their principles of functioning.

The Nordek AWAC (Acoustic wave and current) profiler comprises three technologies to measure and calculate wave and current information: a pressure sensor, three acoustic transducers for current estimation, and an independent vertically-orientated echo-sounder for Acoustic Surface Tracking (AST).

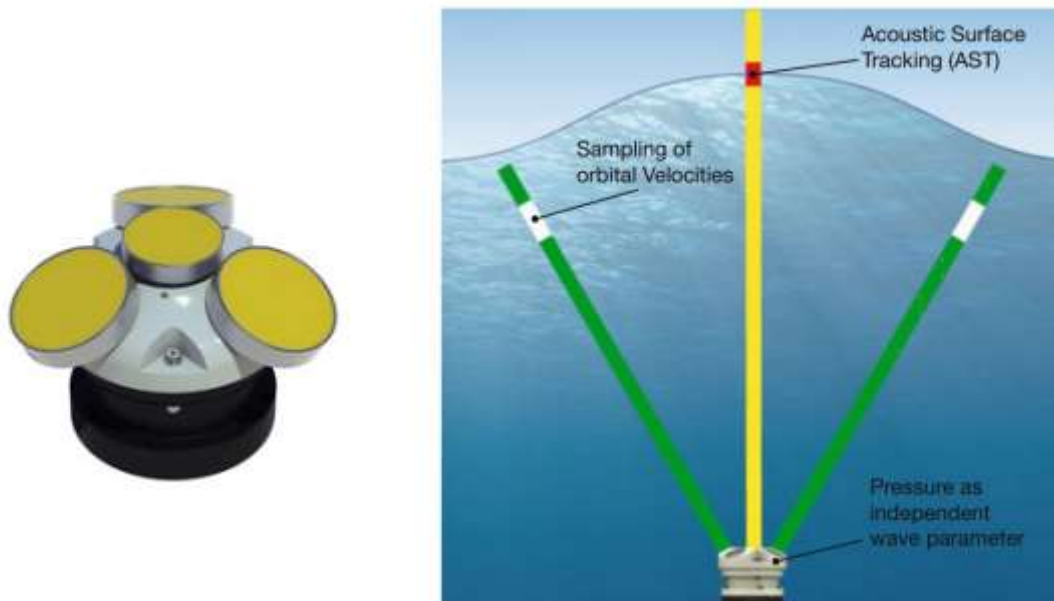


Figure 1: Photo of the Nordek AWAC, and principle of measurements. From the Nordek AWAC brochure.

Wave direction is calculated by combining AST with orbital velocity measurements in an array near the surface. The four-point array data (3 for orbital velocities and one for AST) can be processed with the maximum likelihood method to generate accurate directional wave spectra. It allows users to select the maximum likelihood method or an SUV-based approach for wave calculations (if the AST fails, the redundant pressure measurement can be used). Its output using either method includes the first-5 Fourier coefficients.

AWACs can be used at 600 KHz or 1 MHz, to accommodate different deployment depths. The 1 MHz version has a nominal sampling range for current velocity of 30 meters and waves of 40 meters. The 600 kHz version will sample currents to 50 meters and waves to 60 meters.

The Teledyne RDI workhorse wave array uses four acoustic beams providing a redundant data source in the case of a blocked or damaged beam. It can operate at 300, 600 or 1200kHz. Using up to a total of 12 radial velocity measurements to quantify the near-surface orbital fluctuations at up to three different depth levels as inputs for the directional spectra measurement (ACT, 2012), it allows measuring the multi-directional wave spectra, current velocity profiles, and water level at the same time.



Figure 2: Picture of Teledyne's RDI workhorse wave array. From <http://www.rdinstruments.com/monitor.aspx>.

Birch et al. (Birch, Fissel, Borg, Lee, & English, 2004) presented the results of an intercomparison between the two ADCPs presented above, the AWAC from Nortek and the RDI workhorse wave array. For the study, both ADCPs were deployed at exactly the same location, in the Strait of Georgia near Vancouver. They obtained relatively similar periods and wave heights with both, but noted that the AWAC surface track is more precise than that of the RDI ADCP because of the dedicated narrow vertical beam which has a short acoustic pulse. Surface tracking is however susceptible to false returns from bubble clouds generated by extreme wind-wave conditions or by boat wakes and wash.

2.1.2 Ultrasonic sensors

Ultrasonic transducers are purely non-intrusive sensors as they are to be placed at some distance (of the order of some meters) above the sea water surface. They emit, generally using a piezo electric crystal, bursts of narrow beam of ultrasonic sound waves (of frequency larger than 20 KHz), normally travelling vertically downwards, that reflect off the water surface and return to the sensor. The time interval between the sending and the receiving of the sound wave is converted into distance based on the speed of sound in air. Most sensors now have an internal thermometer in order to compensate for the effects of temperature variations on the speed of sound.

Christensen et al. (Christensen, et al., 2013) obtained one-dimensional wave spectra using an ultrasonic altimeter mounted at the bow of an anchored ship. During three field experiments, they used two kinds of ultrasonic probes, a Banner U-GAGE QT50U with a range of 0.2–8 m, shown here in Figure 3, and a Senix TSPC-21S having a range up to 15 m.



Figure 3: Picture of the Banner U-Gage QT50U.

Motion measurement of the ship motion, provided by a 2D accelerometer or a commercial inertial motion unit, was used to correct wave elevation data. Measurements obtained with this system were comparable to those obtained with a Datawell Directional Waverider Mk III wave buoy, moored in 120 m water depth, as shown by the obtained spectra presented here in Figure 4.

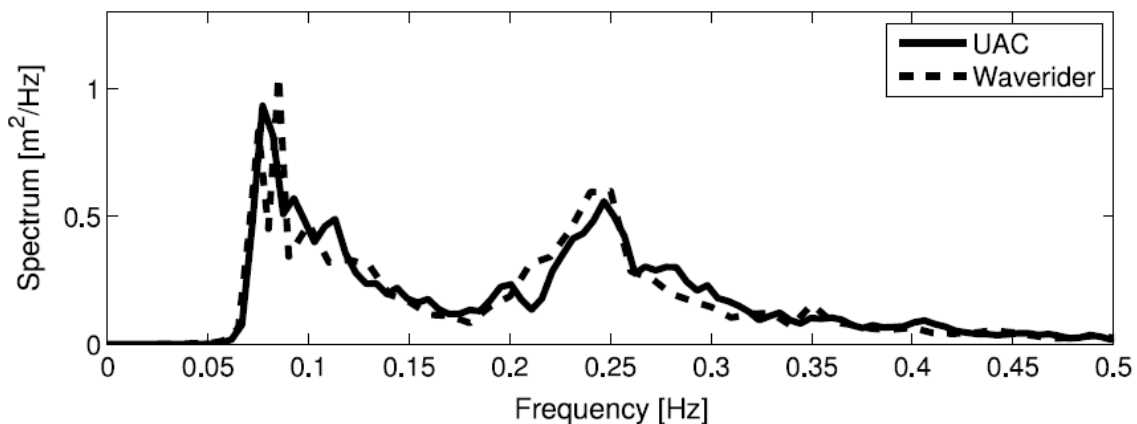


Figure 4: Variance spectrum of the signal from the UAC and from the waverider. From (Christensen, et al., 2013).

They argue that this system, inexpensive and portable, may be particularly useful during field experiments where traditional wave buoys are unavailable, or for coastal surveys. The system can not for the moment be used when the ship is cruising, as data contain some doppler shifts. In this case they obtained strongly biased estimates of peak and mean periods.

2.2 RADAR REMOTE SENSING

Microwave remote sensing of the sea has been extensively researched and developed since the late 1970's, primarily thanks the ability to place sensors on aircrafts and satellites.

Microwave remote sensing, using wavelengths from about one centimeter to few tens of centimeters, enables observation in all weather conditions, unlike visible and infrared remote sensing. There are two types of microwave

remote sensing systems: passive and active. The passive type receives the radiation emitted from objects on the ground. The active type receives the backscattering of the microwaves that it previously emitted. Active radar data is usually preferred as they are independent of daylight and cloud conditions.

The many radar systems developed can be classified according to the frequency band they use. Those frequency bands are illustrated in Figure 5.

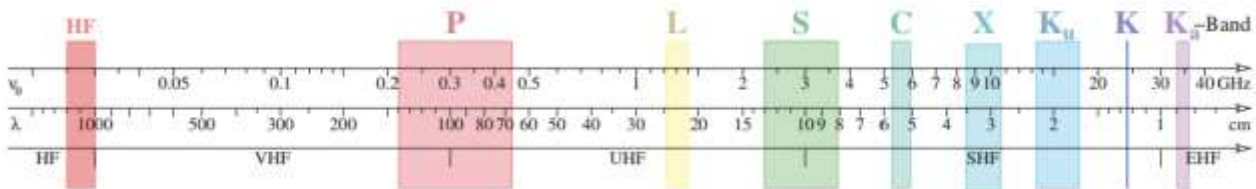


Figure 5: Radar frequency bands. From (COST Action714, 2005)

In this table, the different frequency bands used by the systems are indicated, with the measuring principles and the platforms on which they have been used.

Only a brief overview of some radar systems is presented here. For more details, the reader is referred to the excellent work resulting of the European COST Action 714 (COST Action714, 2005), from which was taken Table 1 presenting various existing radar systems.

2.2.1 Radar altimeters

Altimeters provided a great amount of knowledge of the ocean's bathymetry and topography, and they are now the most widely used source of wave measurements, primarily for validation of global ocean models.

Using radio pulses, they primarily measure the height of the satellite above the sea surface. When this is subtracted from the height of the satellite's orbit, the difference is sea level relative to the center of earth. The shape of the surface is due to variations in gravity, which produce geoid undulations, and to ocean currents which produce oceanic topography, the departure of the sea surface from the geoid (surface of the ocean at rest, which was not well known locally before 2004).

The same altimeters can also be used to measure the wave height. Stewart (Stewart, 2008) explains that the altimeter technique works as follows. Radio pulses from a satellite altimeter reflect first from the wave crests, later from the wave troughs. The reflection stretches the altimeter pulse in time, and the stretching is measured and used to calculate wave height. Accuracy is $\pm 10\%$.

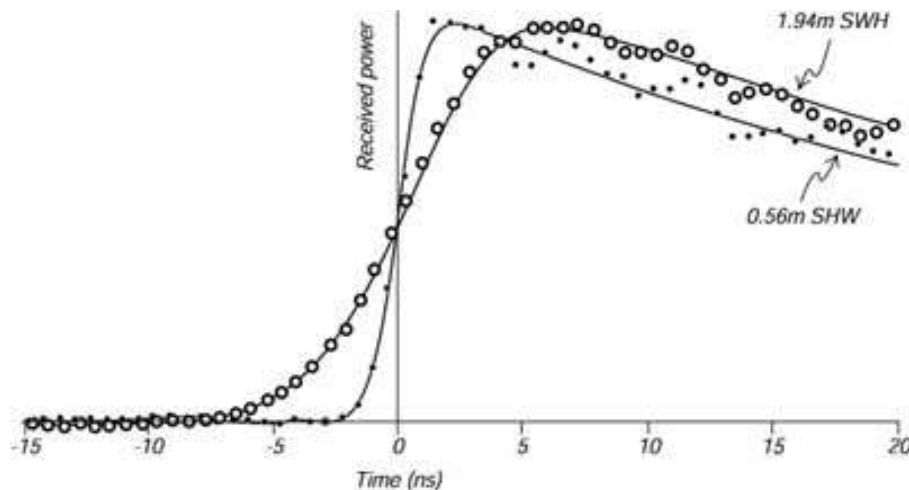


Figure 6: Shape of radio pulse received by Seasat altimeter, showing the influence of ocean waves. The shape of the pulse received is used to calculate wave height. From (Stewart, 1985).

The use of altimeter data to study the wave climate started with the launch of GEOS-3 in 1975, but it is only with Seasat in 1978 that the first picture of the wave climate of the whole globe was obtained. Later satellites equipped with an altimeter include Geosat from 1985 to 1988, ERS-1 & 2 from 1991, Topex/Poseidon from 1992 to 2001, Jason1 from 2001, and Jason2 in 2008. Topex/Poseidon and Jason were specially designed to make extremely accurate measurements of sea-surface height, measuring sea-surface height with an accuracy of ± 0.05 m. Altimeter data were used to produce monthly mean maps of wave-heights and the variability of wave energy density in time and space.

Challenor et al. (Challenor, 2008) concludes that our knowledge of the wave climate has been revolutionised by the advent of radar altimeter data. For the first time we have a truly global picture of what the wave climate is doing. The major contribution has undoubtedly been with regard to changes in significant wave height and their relationship to phenomena such as the NAO. Recent work on deriving wave period and skewness from radar altimeter data opens up new possibilities in studying the global wave climate.

2.2.2 Synthetic Aperture Radars (SAR)

SAR is a method using a radar system in motion to increase its accuracy. It is a unique sensor for ocean wave measurement from space, with high spatial resolution and no dependency on cloud and light conditions. It uses only one antenna, but since it is in motion, its changing position through time duplicates the effect of several physical antennas spread out in a virtual row. The finely detailed imagery of the oceans surface from a SAR is assuredly the most complex and least understood data provided by remote sensing instruments (<http://www.sarusersmanual.com/>).

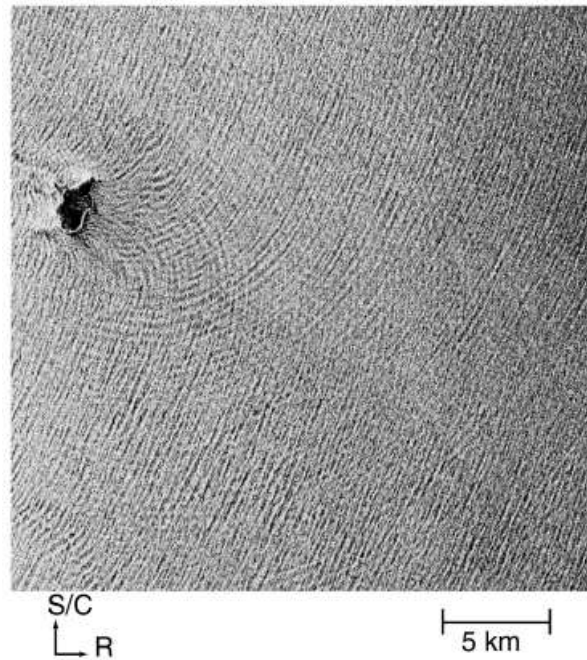


Figure 7: SAR image of ocean surface waves; Range-travelling waves refracting around Santa Barbara Island (taken with RADARSAT-1, on the 25th of November 1998); From (Jackson & Apel, 2004), chap. 2.

The sea surface can appear featureless or contain the signatures of such diverse phenomena as surface and internal waves, upwelling, current boundaries, shallow water bathymetry, wind, rainfall, roll vortices, convective cells, storms, and a wide variety of sea ice forms.

SAR imaging of the ocean surface has had many applications. Holt (Jackson & Apel, 2004) mentions for example that the directional ocean wave spectra derived from SAR imagery has provided information on the spatial evolution of regional and global wave fields, wave fields generated by storms and hurricanes, and wave refraction through currents and eddies. It has also been used to improve wave prediction through assimilation of SAR wave spectra into wave forecast models. Two main problems limiting the accuracy of SAR measurement of ocean waves are the rough estimation of the real aperture radar modulation transfer and the need for some information about the high frequency of the two-dimensional wave spectrum, or wind vector, obtained using a scatterometer.

Other techniques employing radars have been derived from SAR. Ocean waves have been measured for example with interferometric SAR (InSAR). InSAR systems use two antennas. Their measurements are based on the phase difference of the radars signals coherently recorded by both antennas. Along-Track InSAR (AT-InSAR) use two antennas aligned in the platform flight direction. Its major advantages over SAR measurement are the opportunity to measure directly the dynamical motions of the ocean's surface and its low dependency on the RAR modulation transfer function.

A summary of different radar systems used for ocean wave measurements is shown in Table 1, with their respective frequency bands, measuring principles and platform

Research studies and developments in radar remote sensing of the sea are numerous and could be the subject of a large document. Recent state-of-the-art is reported in (COST Action714, 2005). For more details on remote sensing of the ocean using SAR imaging, the reader is referred to the online SAR Marine user's manual (<http://www.sarusersmanual.com/>), or to the books from Robinson (Robinson, 2004) and Martin (Martin, 2014).

Instrument (section)	Acronyms (selection)	Frequency Band	Measuring principle	Platform
Scanning altimeter (5.2)	SRA, SCR	Ka	Topographic map from accurate distance measurements	Aircraft
Marine Radar (5.3)	WAMOS	X	Backscatter modulation at large incidence angles	Ship, coast
Platform Doppler Radar (5.4)	MIROS	C	Backscatter from moderate incidence angles	Ship, platform
HF radars (5.5)	WERA, Pisces, CODAR	HF	Power spectrum of backscattered signal due to moving waves with range and azimuth discrimination	Coast
Non-Doppler Real Aperture Radar (5.6)	RESSAC, STORM, SWIMSAT	C, Ku	Backscatter modulation measured at moderate incidence angles, over 360° in azimuth	Aircraft, satellite (project)
Doppler Real Aperture Radar (5.7)	CORAR	X	Doppler velocity modulation in across-flight direction	Aircraft
Synthetic Aperture Radar (5.8,5.9)	SAR	X,C,L	Travel time (across track) Doppler history (along track)	Aircraft, satellite
Interferometric Synthetic Aperture Radar (5.8,5.9)	INSAR	X,C,L	Two SAR antennas in an along or across track configuration	Aircraft, shuttle, satellite (project)

Table 1: Overview of different radar systems; From (COST Action714, 2005)

Radar remote sensing can be used for ocean wave measurement over smaller areas. Marine radars are used on platforms, aboard ships and from coastal sites. The next sections present the work made by two Marinet partners involved in experimental field testing of MRE. These works deal with the measurement of ocean waves using radars over an area surrounding and enclosing an experimental field test site for MRE.

2.2.3 Marine radars

Under various conditions, signatures of the sea surface are visible in the near range of nautical radar images (< 3 nm) and are known as sea clutter. They are undesirable for navigational purposes and are generally suppressed by filter algorithms. The sea clutter is created by the backscatter of the transmitted electromagnetic waves from the

short sea surface ripples, which are in the range of *cm*. Longer waves modulate the sea clutter signals and therefore become visible in the radar images.

Since standard nautical X-band radar systems (using radio waves between 8 and 12 GHz as specified by IEEE standard 521-1984 - Letter Designations for Radar-Frequency Bands) allow scanning the sea surface with high temporal and spatial resolution, they are able to monitor the sea state in time and space. With each radar antenna revolution, the sea surface is scanned by electromagnetic waves. The received backscatter intensity from the sea surface is transferred via an isolated buffer to the AD converter in a PC. In the WaMoS II system, the data is stored and the wave analysis is carried out. One WaMoS II measurement consists of the acquisition of several radar images (default is 32 images) for its analysis. The resulting wave information, including individual wave spectra and time series of the main statistical wave parameters, are stored and displayed on the WaMoS II GUI.

An OceanWaves GbmH *WaMoS®II* Wave Monitoring System (WaMoS) has been installed at both EMEC substations, situated at Billia Croo (058° 58.322N 003° 21.033W) to cover this wave test site area and on the island of Eday (059° 09.969N 002° 48.165W) to provide coverage of the Fall of Warness tidal test site area. Both monitoring systems consist of a dedicated Windows PC+PCI Interface card, and are fed with data from a marine radar system: a Furuno FAR-21x7-BB series radar at Billia Croo and a Kelvin Hughes *MANTA 1700* at Eday. These marine X-band radars operate continuously, taking site-wide sea state measurements based on the backscatter of microwaves from the sea surface.

The next sections describe the result of the work recently done at EMEC in comparing WaMoS II radar data with data from wave buoys and ADCPs.

2.2.3.1 Radar/Waverider buoy comparison

This section will compare wave measurements from the marine radar with wave measurements from the three Datawell Waverider MKIII buoys currently deployed at the Billia Croo wave site.

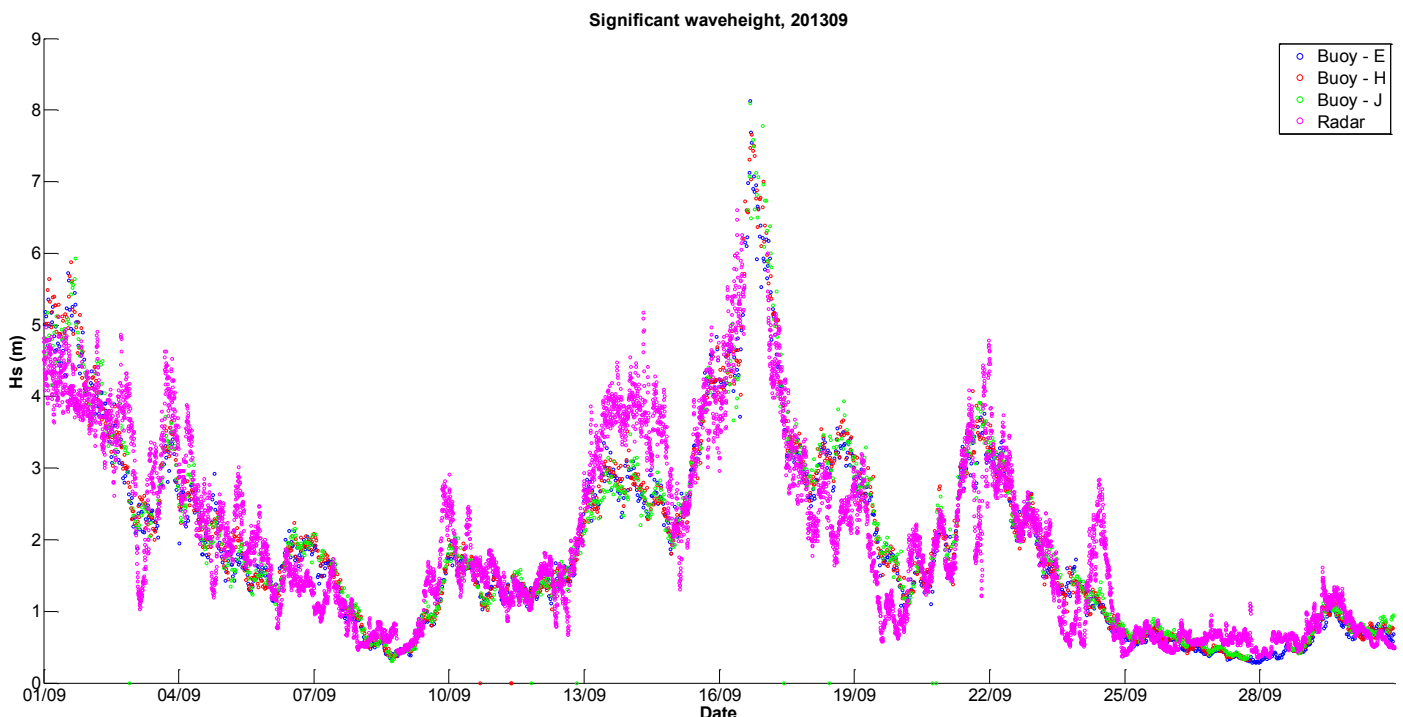


Figure 8: Radar and waverider significant wave height comparison, September 2013

The time series displayed in Figure 8 above show the observed significant wave heights for each of the three Datawell Waverider buoys currently deployed at the Billia Croo wave test site (blue, red and green plots) and the observed significant wave height for the Billia Croo marine radar system (magenta plot).

During this period, the observed records from the two sources are reasonably consistent. There are however some small periods of inconsistency – namely around 14-15/09 and around 17/09. These differences may be due to the nature of the measurement methodology: the Waverider buoy provides a point measurement of the wave parameters while the marine radar system provides a spatial average over the entire observation area.

For both systems, the significant wave heights are calculated from the spectral wave characteristics: $H_s = 4\sqrt{m_0}$ where m_0 is the zeroth spectral moment.

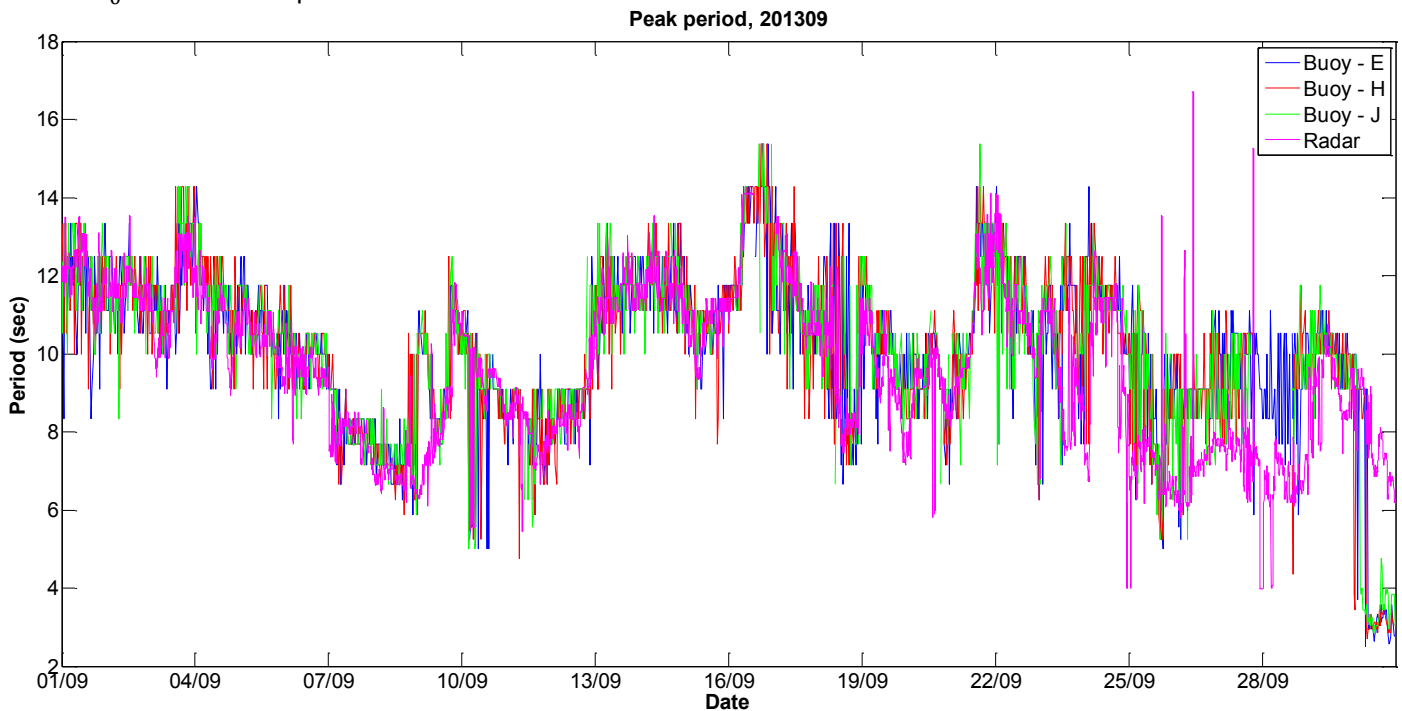


Figure 9: Waverider buoy and marine radar peak period comparison

The peak period is defined as the inverse of the frequency at which the spectral power is maximal: $T_p = \frac{1}{f_p}$, where f_p is the “peak” frequency. This parameter is displayed in Figure 9 where it can be observed that the values of T_p from both systems are reasonably consistent.

It is worth noting that the two systems measure the wave spectra over different frequency ranges with different frequency subdivisions. The Waverider buoys use the frequency range of 0.025 Hz to 0.58 Hz with a frequency subdivision of 0.005 Hz up to 0.1 Hz and a subdivision of 0.01 Hz from 0.01 Hz to 0.58 Hz. The marine radar system uses a frequency range of 0.0055 Hz to 0.35 Hz with a frequency subdivision of 0.0055 Hz. This difference in frequency ranges and subdivisions may be the cause of the slight differences in the datasets.

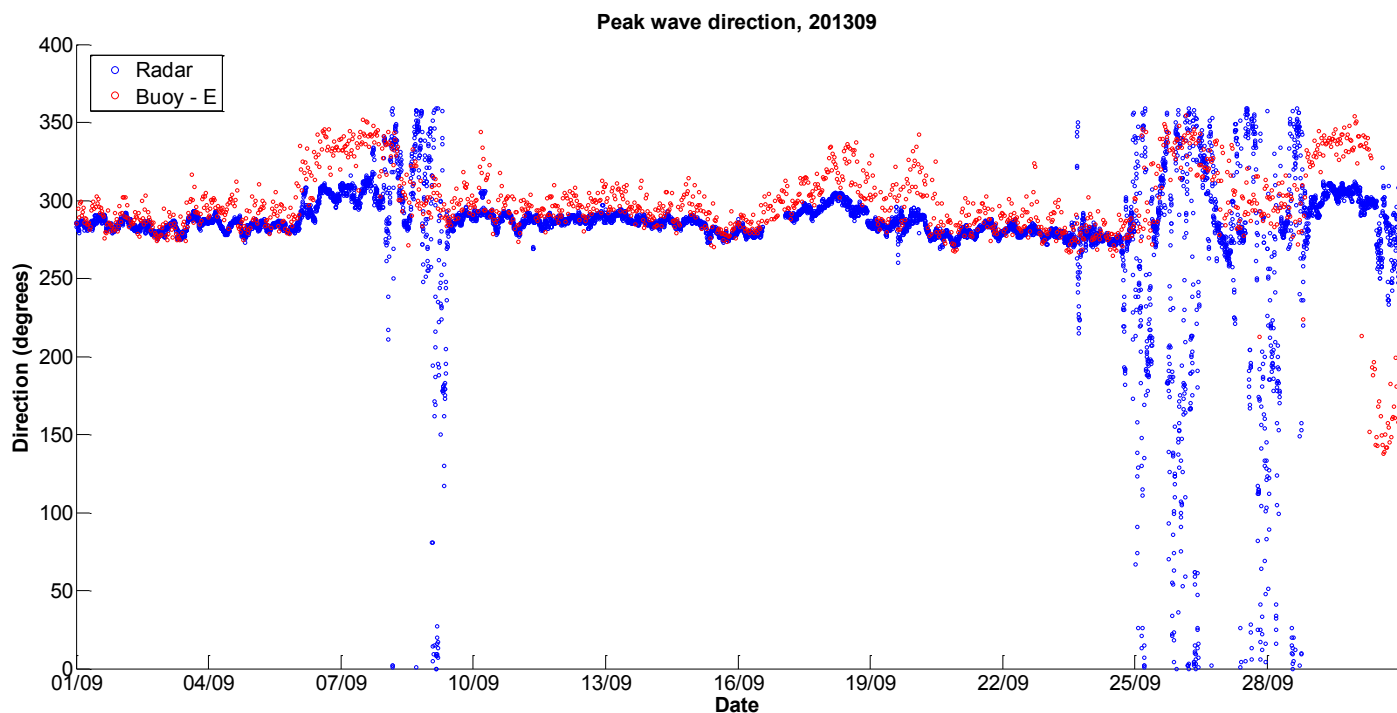


Figure 10: Waverider buoy and marine radar peak wave direction comparison

The peak wave direction is defined as principal direction of the frequency at which the spectral power is maximal, f_p as defined in the previous section. This parameter is displayed in Figure 10 where it can be seen that there is a good degree of consistency between the measurements from the two systems.

There are however several periods where the directions are divergent, namely around 09/09 and between 25/09 and 29/09.

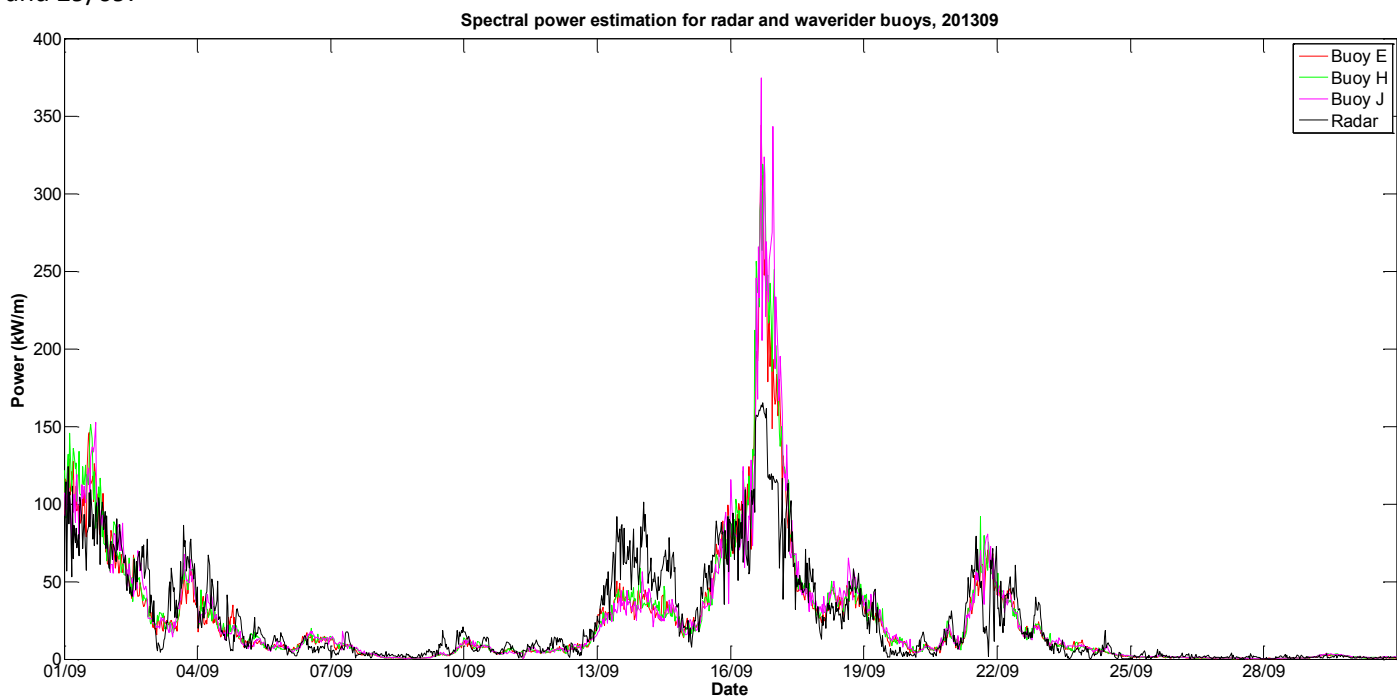


Figure 11: Waverider buoy and marine radar spectral power estimation

The preferred method of power calculation adopted by EMEC is that described by (Pitt, 2005):

$$P = \rho g \int C_g(f) S(f) df$$

In practical terms this can be considered as the power in the waves from all directions, or simply as the power were the wave system unidirectional. It is calculated without reference to the wave spectral direction (ϑ) using:

$$P = \rho g \sum_{i=1}^{i=64} S_i C_g(f_i) \Delta f_i$$

In this case, $V_g(f_i)$ is the group velocity at the i^{th} frequency, S_i is the corresponding spectral density estimate, Δf_i is the i^{th} frequency subdivision, ρ is the density of seawater (1025 kg/m^3) and g is the acceleration due to gravity (9.818366 m/s^2).

2.2.3.2 Radar/ADCP comparison

This section compares now wave measurements from the WaMoS II marine radar with wave measurements from an RDI Workhorse 600 kHz ADCP deployment. The nature of the bathymetry and currents at the tidal test site are such that the conditions vary widely across the site. As such, only wave data from the radar cartesian measuring box number 3 will be used in the comparison as this box covers the area that the ADCP was deployed in. It is also worth noting that the radar system in place during the period of the ADCP deployment was uncalibrated and should be viewed with caution.

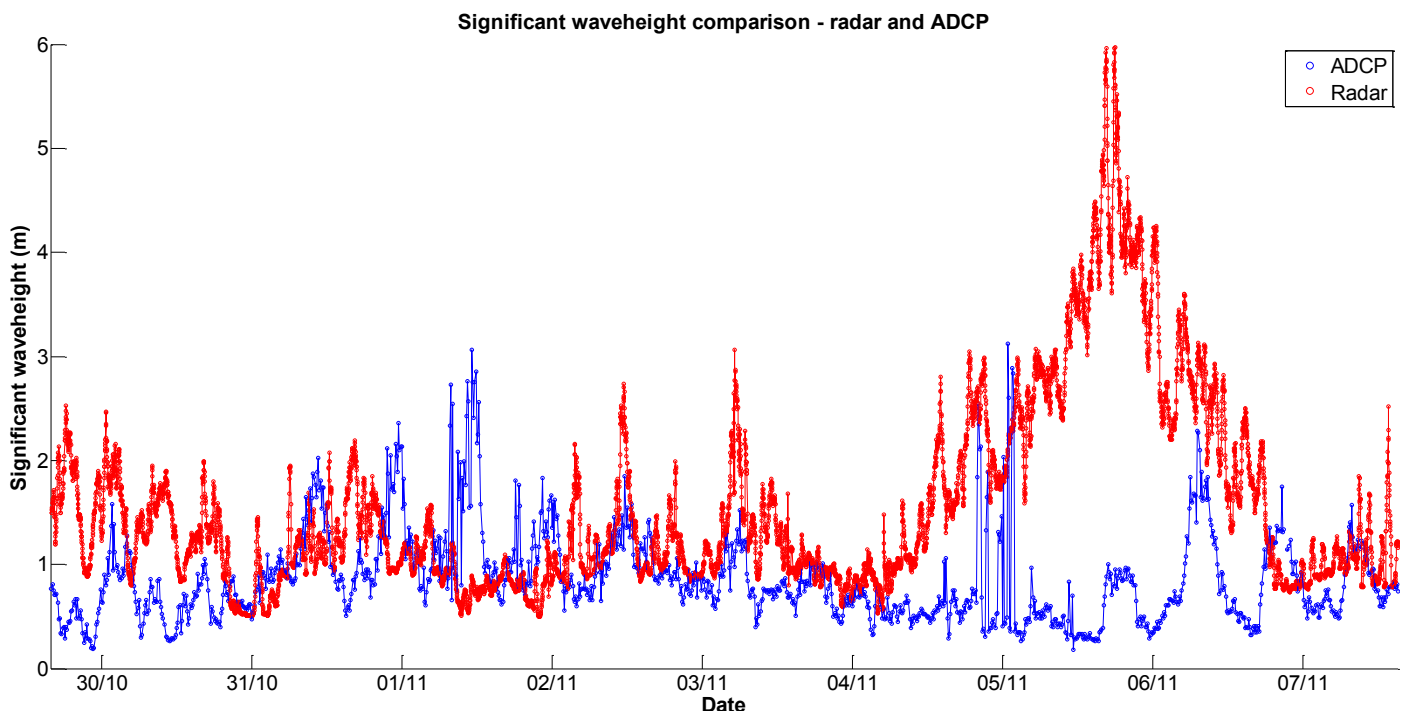


Figure 12: Comparison of significant wave heights obtained from ADCP and marine radar.

The significant wave heights displayed in Figure 12 are representative of the wave conditions at the south end of the Fall of Warness tidal test site during the period 2012/10/30 – 2012/11/08. A reasonable agreement can be observed at the beginning of the period, with an obvious divergence from 2012/11/04 onwards.

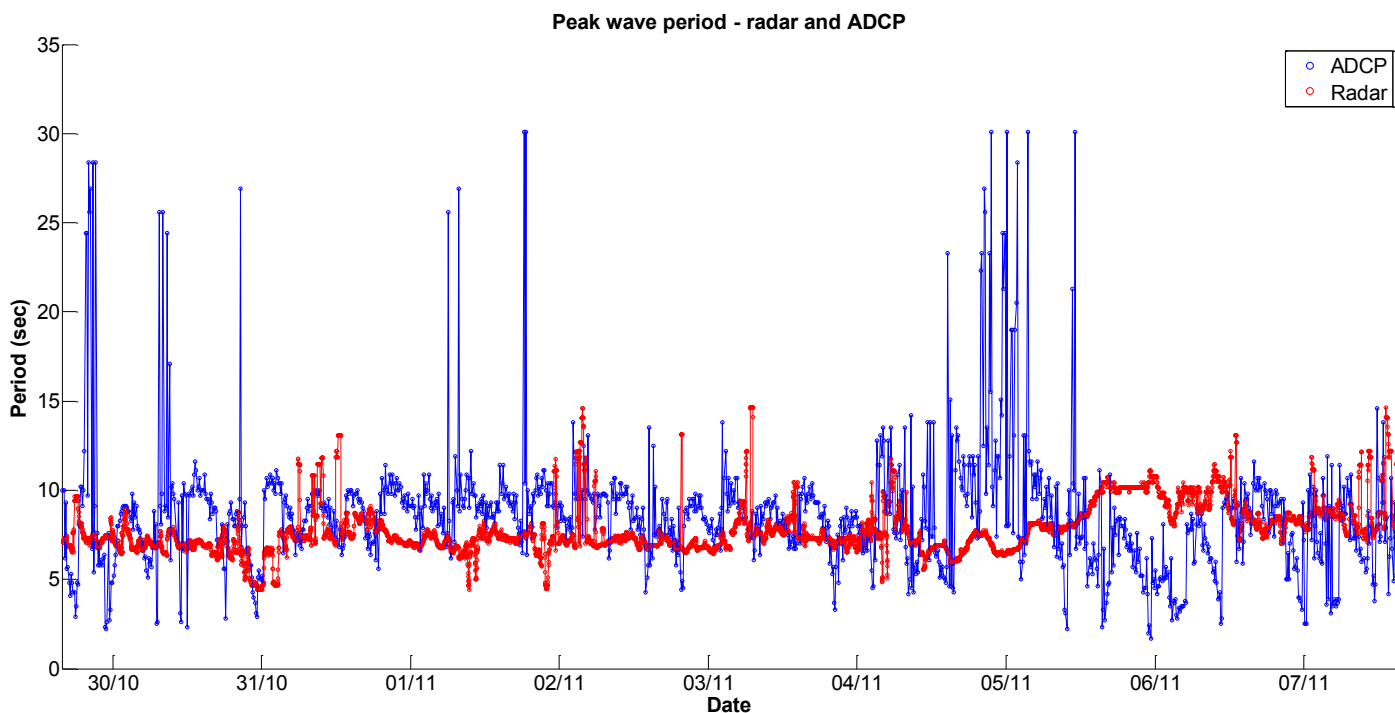


Figure 13: Comparison of peak wave periods obtained from ADCP and marine radar.

The peak wave period comparison is displayed in Figure 13 above, and a relatively good correlation can be observed throughout the survey period. Some unreasonably high spikes in the ADCP data are observed, especially around 2012/10/30 and 2012/11/05. It can be concluded with reasonable confidence that these spikes are not representative of actual sea conditions on the site and are in fact erroneous measurements.

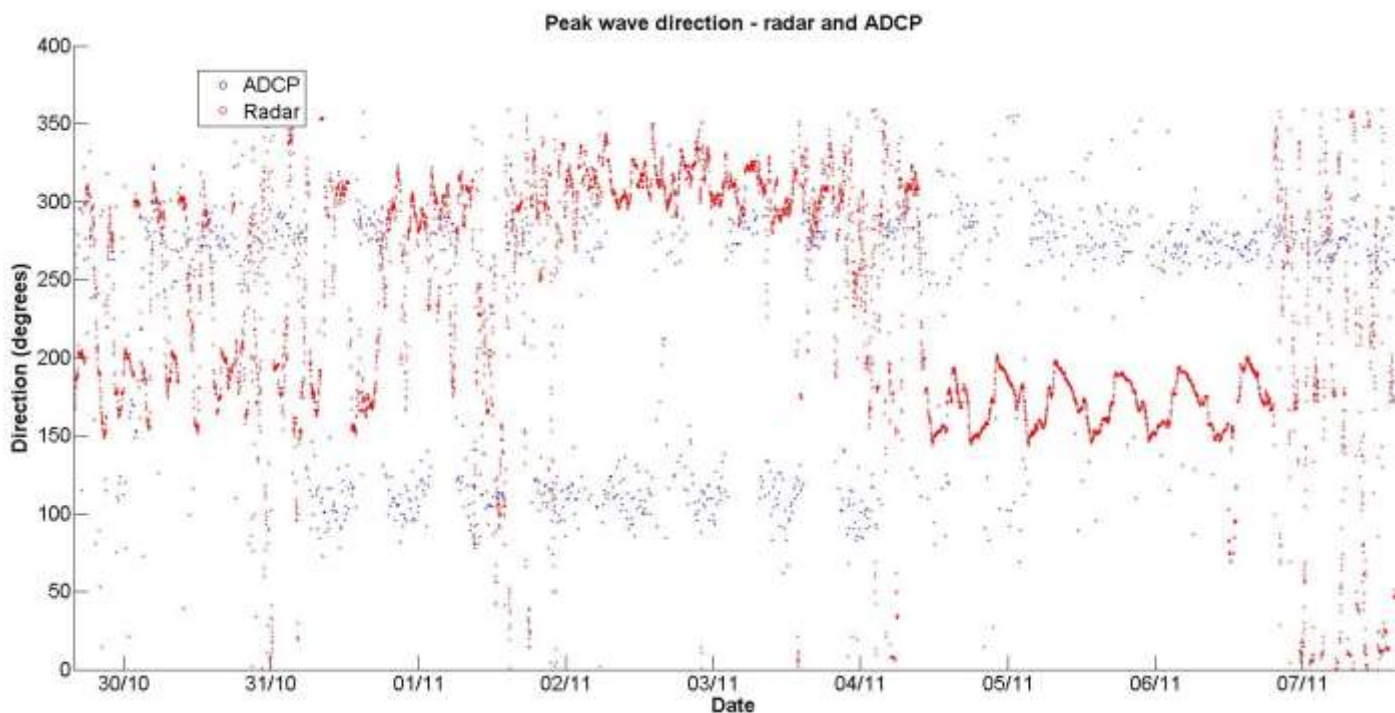


Figure 14: Comparison of peak wave directions obtained from ADCP and marine radar.

The peak wave direction comparison is displayed in Figure 14 above. There are periods of reasonable correlation, particularly between 2012/11/02 and 2012/11/04, but in general there is low correlation between the two sources. A

possible cause of this is that the marine radar system provides a spatial average over a relatively large sea area while the ADCP provides a point measurement within that same radar area. This, combined with the high level of spatial variability, may be the cause of the poor comparison.

2.2.4 HF radar

High frequency (HF, 3-30 MHz) ground wave radars are shore-based remote sensing systems that transmit vertically polarised electromagnetic waves, which due to the conductivity of the sea surface propagate long distances with very little loss. As they travel, they interact with the rough sea surface, which acting as a diffraction grating scatters them in all directions with some scattered back to the radar receivers (Kahma et al., 2005).

Figure 15 shows a typical radar backscatter spectrum, also referred to as Doppler spectrum, obtained after processing the backscattered signals recorded at the receivers. It consists of two distinctive peaks located on either side of the radar transmission frequency and four continuous sidebands surrounding them.

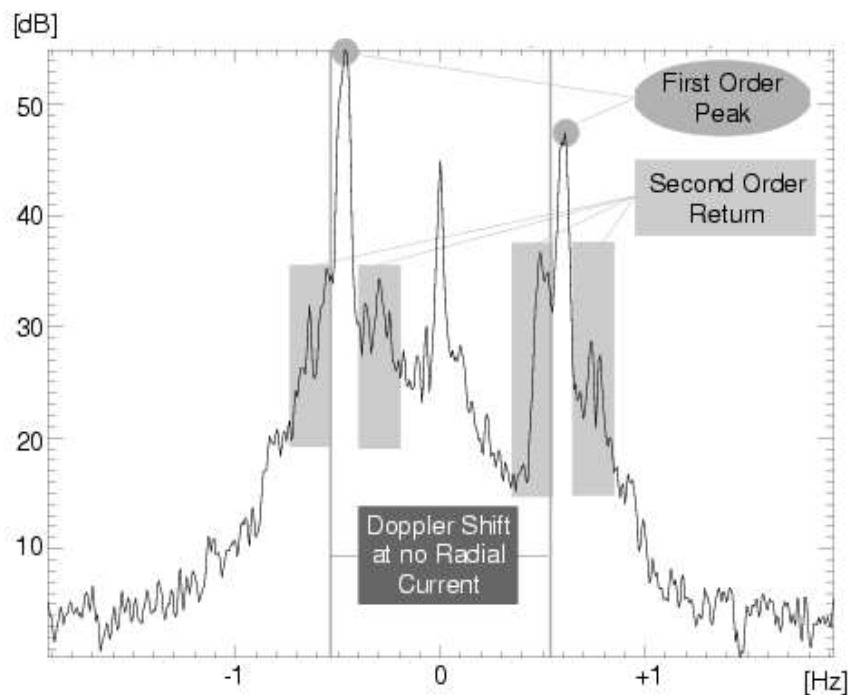


Figure 15: HF radar Doppler spectrum; From (Gurgel et al., 1999)

The two primary peaks in Figure 15 are generated by the coherent reflection of the electromagnetic waves from ocean waves with half the transmitted radio wavelength. Resonant Bragg scattering is the dominant mechanism governing the backscatter process (Gurgel et al., 1999), hence these peaks are often referred to as the Bragg peaks. The frequency at which these appear on the Doppler spectrum depends on the combined effect of the phase velocity of the scattering waves and the radial current speed,

$$\omega_D = \pm\omega_B - 2k_0u$$

where ω_D is the Doppler frequency of the scattered wave, ω_B is the angular frequency of the Bragg scattering ocean wave, k_0 is the radio wave number and u is the radial current speed. The sign in front of ω_B depends on the direction of the scattering wave, positive if travelling towards the radar and vice versa. Because u is the only unknown in the above equation, this can be used to derive the surface current velocity. Wind direction can be inferred from the relative height of the two Bragg peaks (see Fernandez et al., 1997, Wyatt et al., 1997), while the rest of the spectrum, consisting of a continuum due to non-linear wave interactions and scattering processes along with a noise floor (Kahma et al., 2005), can be used to extract information about the directional ocean wave spectrum.



Figure 16: Picture of the SeaSonde. From <http://www.codar.com/SeaSonde.shtml>

The SeaSonde is one of the leading HF radar systems on the market. Designed and built by US company Codar, the SeaSonde maps ocean currents and wave fields in real time. It offers three configurations: Long-range, High-resolution or standard mode.

In long-range mode, the instrument can provide measurements up to 220 km offshore, with a resolution of 3 to 12 km, using radio waves between 4.3 and 5.4 MHz. The range in high-resolution mode, using radio waves between 27 and 45 MHz, is decreased to a maximum of 30 km, with a resolution of up to 200 m.

The WERA system (which stands for Wellen Radar (Gurgel, Antonischki, Essen, & Schlick, 1999)), is another leading HF radar system, made by German company Helzel. It can also operate at very low frequencies (5 MHz) to provide very long ranges or at the upper HF band (30 MHz) with a resulting range of 50 km. The VHF WERA, operating with radio waves of frequencies up to 50 MHz, provides high resolution of 100 m for ranges of up to 20 km. The WERA system can be operated with multiple antennae, in order to resolve the waves' direction of propagation.

2.2.4.1 Wave inversion techniques

The scattering theory that underpins wave measurement with HF radar is based on a perturbation analysis of the interaction between electromagnetic and oceanic waves. A detailed description of this theory and the derivation of the fundamental equations can be found in (Barrick D. , 1972), (Barrick & Weber, 1977) and (Weber & Barrick, 1977). The first-order solution of the perturbation expansion describes the occurrence of the aforementioned Bragg peaks, which are therefore often referred to as first-order peaks. To second-order, the solution describes the continuum surrounding those peaks, which is the result of the combination of hydrodynamic non-linear interactions (hydrodynamic effect) and double scattering (electromagnetic effect). The hydrodynamic second-order scatter results from a single scatter off a second-order ocean wave generated by the interaction of two fundamental ocean waves with wave vectors k_1 and k_2 . On the other hand, the electromagnetic second-order scatter occurs when the incident radar wave is scattered by a first-order ocean wave whose wave vector is k_1 , which is itself scattered again by another first-order ocean wave of wave vector k_2 (Zhang, Walsh, & Gill, 2012). The only constraint for a valid reflection to occur is that the result after vector summation has to satisfy the Bragg resonance condition, hence $k_1 + k_2 = -2k_0$ in the direction along the radar beam. Multiple combinations are possible and consequently, the second-order part of the spectrum is a representation of the full directional ocean wave spectrum.

The integral defining these processes and hence relating the scattered power spectrum to the ocean directional spectrum is a non-linear first kind Fredholm equation (Kahma, et al., 2005). The different techniques that have been developed to invert this integral into a meaningful directional spectrum, either try solving the non-linear problem directly (Hisaki, 1996); (Hashimoto & Tokuda, 1999)), or apply linearising techniques before (Lipa, 1977); (Wyatt,

1990); (Howell & Walsh, 1993)). From all the different approaches, Wyatt's (1990) method, which is distributed with the Seaview Sensing software package (www.seaview Sensing.com), is the only one that has proven to have the speed and robustness required to be applied operationally. The algorithm first removes the non-linearity in the integral to then integrate using an iterative scheme, which modifies the wave spectrum within each iteration loop according to the difference between the measured and integrated Doppler spectra. The iterative scheme is initialised with a Pierson-Moskowitz spectrum and a model for the directional distribution. The spectral shape of the initial Pierson-Moskowitz spectrum is determined using significant wave height and mean period extracted directly from the radar spectra (Wyatt, et al., 1985). A discussion on the applicability of this method to calculate wave power is provided in (Wyatt, 2007). Correlations of 0.91, 0.75 and 0.92 are reported for significant wave height, energy period and wave power radar/buoy comparisons, respectively.

Empirical expressions relating the backscatter spectrum to the equivalent ocean wave spectrum or some of its summary parameters have also been produced (i.e. (Barrick D. , 1977); Wyatt 1988, 2002; Maresca and Georges 1980; Heron and Heron 1998, (Essen, Gurgel, & Schlick, 1999); (Gurgel, Essen, & Schlick, 2006)). Although such relationships do not allow for the estimation of the full directional spectrum, some of them have proven to be robust methods for the estimation of significant wave height. The results of a calibrated version of an expression developed by Barrick (Barrick D. , 1977) to retrieve significant wave height have been used to observe the wave energy evolution in coastal areas (Ramos et al., 2009), study the wind speed dependence of the retrievals (Haus et al., 2010) or the spatial variability of waves interacting with an estuarine outflow (Haus et al., 2006). These publications report correlations that range from 0.7 to 0.86 and root-mean-squared errors of the order of 0.2-0.3 m. Essen et al. (1999) found the second-order part of the spectrum to be strongly correlated with the significant wave height weighted by an azimuthal function, and used this relationship to invert the radar power spectrum into significant wave height. A similar approach is applied in the algorithm provided with WERA radars (Gurgel, Essen, & Schlick, 2006). Assuming that the measured radar spectrum depends on the wave height spectrum obtained with a wave buoy and weighted by an angular spreading function, the authors determined a set of frequency-dependent regression coefficients that allow inferring ocean wave spectra from second-order Doppler spectra.

2.2.4.2 Plymouth University radar system

A WERA HF radar (Gurgel, Antonischki, Essen, & Schlick, 1999) has been installed in the north coast of Cornwall to overview the Wave Hub test site area. It is the first application of this new remote sensing technology to resource characterisation and environmental monitoring for marine renewable energy installations and, as opposed to the majority of the HF radars installed worldwide, optimised for surface current measurement, it has been specifically configured for wave measurement.

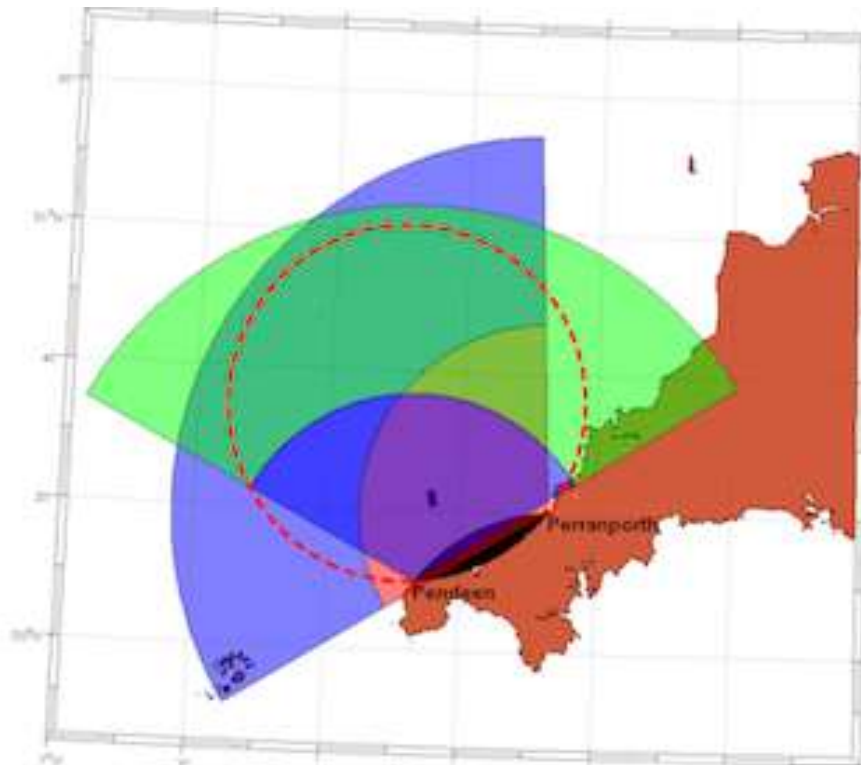


Figure 17: Map showing the positions of the two HF radars on the north coast of Cornwall. From the Marinet website.

The two radar stations that compose the system, located at Pendeen (master station) and Perranporth (slave station) have been operational since the end of 2010 and beginning of 2011, respectively. Both operate at a centre frequency of 12 MHz, and make independent measurements for 17 minutes every hour, which are then available on a 75-by-90 km grid with 1 km spacing.

The received backscatter signals are processed in near real time using two different algorithms. Provided the two radar stations are operational and retrieving good quality data, the Seaview Sensing software generates an estimation of the directional wave spectrum for each point on the grid, while the in-house WERA software provides the omnidirectional frequency spectra and the mean wave direction at the same locations. Due to the radial nature of HF radar measurements, there is a direction ambiguity when the results are calculated using data from one station only. Consequently, if dual information is not available only the non-directional results are provided.

2.2.4.3 Radar/buoy comparison

The empirical algorithm included in the WERA software has been re-calibrated (see (Lopez, Conley, Magagna, & Greaves, 2013)) using data collected at the Wave Hub with a SeaWatch Mini II directional buoy deployed at 55m depth. The buoy measures the water surface elevation at a sampling frequency of 2 Hz during 17 min and 4 s, every 30 min. A period spanning almost one month, from the 11th of August to the 4th of September 2012 was used for the calibration. The wave climate measured by the buoy over this period varied between values below 0.3 m and above 5 m. A second dataset, containing almost three month's worth of data was then used to help verify the wave height estimations obtained when applying the new in-situ adjusted parameters. The results of such validation are presented hereunder.

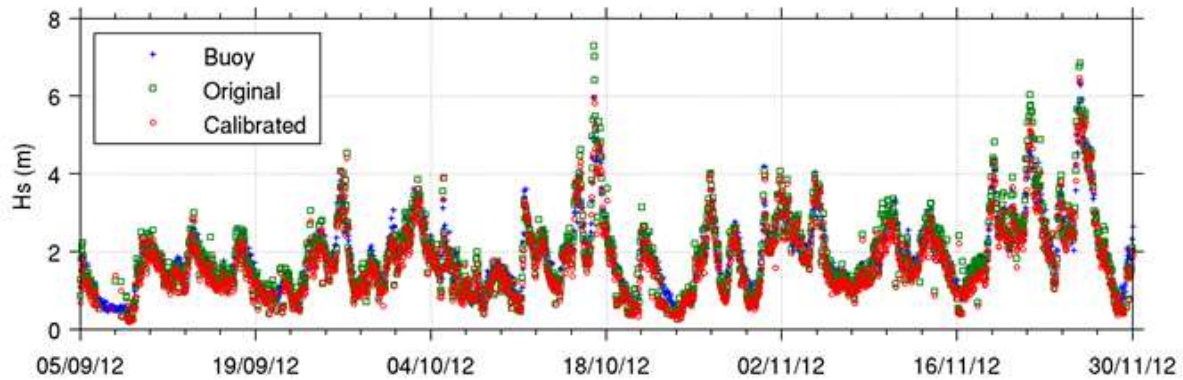


Figure 18: Time series of radar significant wave height calculated with the original and local calibrations and in-situ-measured wave height (September 2012 – November 2012).

Figure 18 displays the significant wave height calculated as four times the square root of the zeroth spectral moment. The agreement between radar and buoy wave height is very good throughout the two months depicted in the figure. The most noticeable effect of the local calibration (red open circles) is a better agreement with the in-situ measurements at the most energetic events, most remarkably around the 17/10, when the un-calibrated algorithm produces an approximative 2m overestimation in wave height.

2.2.4.4 Spatial comparisons

Radar/in-situ comparisons

Validation of HF radar wave measurements has generally been based on the comparison with data acquired at a single point, located in the middle of the radar measurement region where the highest quality data are expected, and therefore provides little insight about the spatial reliability of the measurements. Here, we provide radar to radar comparisons at the locations of two in-situ instruments, to then compare the results of both measuring systems.

The scatter plots displayed in Figure 19 show the correlation between measurements collected at two sites located 12 km apart, which correspond to the deployment coordinates of a Seawatch Mini II wave buoy (50.34°N, 5.60°W) and a RDI Workhorse ADCP (50.32°N, 5.44°W). It is worth noting that while the scatter on the radar to radar comparison (left panel) is higher, the equations resulting from the regression are very similar in both plots. It seems to be safe to assume that both radar and in-situ instruments measure the same variability between two distant locations and that the smaller correlation and higher scatter in the radar comparison is mainly a result of the measurement technique. While both wave buoy and ADCP result in point measurements, the radar provides a spatial average over a square kilometer area, hence the results are foreseen to have higher scatter.

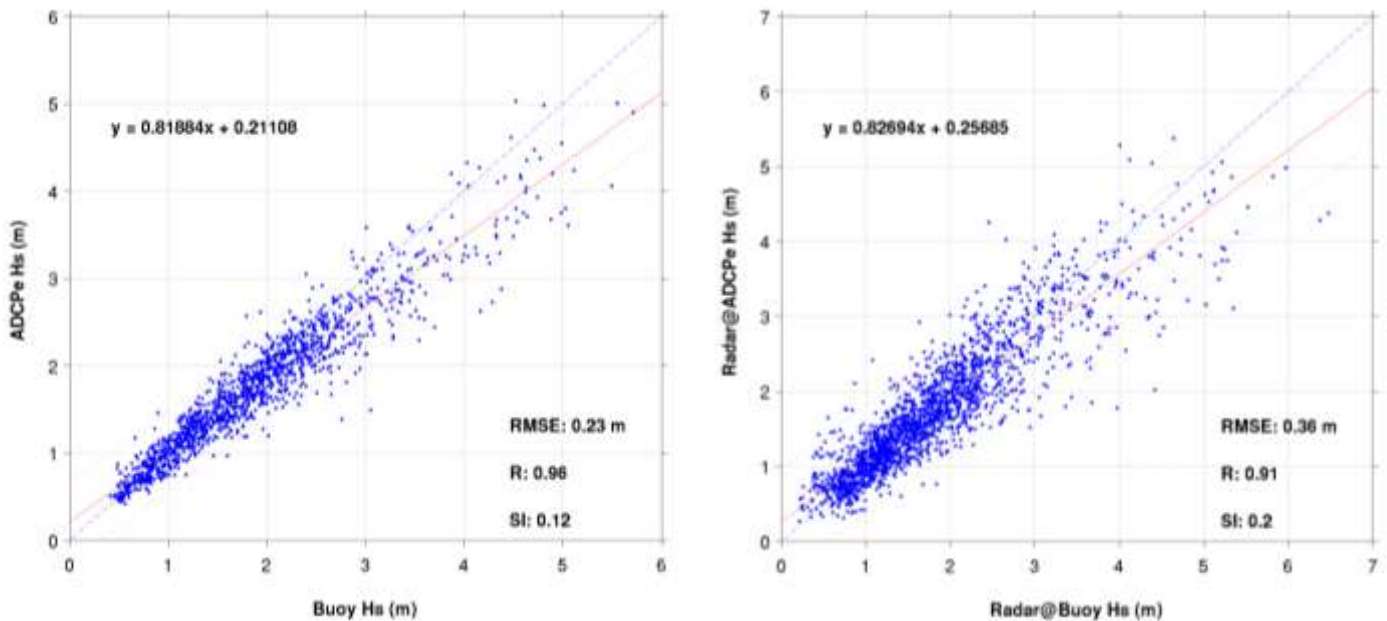


Figure 19: Significant wave height comparison at two distant locations (September 2012 – November 2012). Left panel: Significant wave height as observed by a SeaWatch Mini buoy and a RDI Workhorse located 12 km apart. Right panel: Significant wave height as observed by the HF radar at the buoy and ADCP locations. The blue dashed line is the 1:1 slope and the solid red line is regression best fit. The equation of the regression and some statistical error measures are also shown.

Radar/model comparisons

Wave models constitute a source of spatial data which can shed light into the spatial reliability of HF radar wave estimations. We have compared the results of the radar system to the products of the HOMERE database (Boudière, et al., 2013), generated at Ifremer to support research activities related to the development of marine renewable energies. The database is a 19-year hindcast, covering the period 1994-2012 and obtained with the Wave-Watch III (WW3) wave model on a refined unstructured grid whose resolution ranges from 200 m to 10 km. Those grid points located within the radar coverage area not further than 500 m from a radar grid point have been used for comparison.

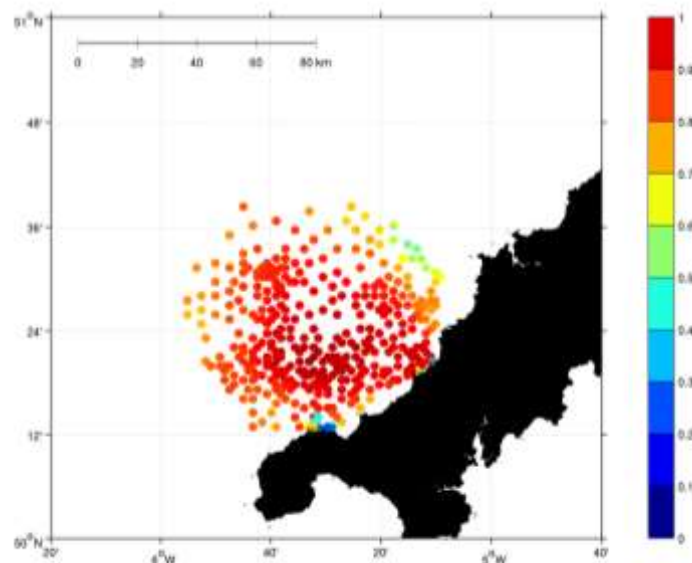


Figure 20: Correlations between data from WW3 and measurements from HF radar, made using the significant wave height (September 2012 – November 2012).

Comparison of significant wave height estimates obtained with the wave model and the radar is depicted in Figure 20. A very good correlation (above 0.8) can be observed at most of the studied locations. Few points, located near the coast constitute the only disagreement between radar and model. These are in areas where the radar beams from the two stations intersect each other almost parallel and this situation is expected to produce lower quality data. However, as of beginning of July, Ifremer detected a problem with the current and water level used as forcing fields that can affect the model results, especially in coastal areas. These results have to therefore be considered with caution. Nevertheless, the good correlations point to the radar results as reliable spatial estimates of significant wave height.

2.3 IMAGING METHODS

2.3.1 Stereo-photogrammetry

Photography seems too be an obvious technique to observe and record water waves. With stereo-photography, a three-dimensional image of the surface can be obtained. The technique for measuring water waves is similar to that used in terrestrial topography. Due to the dynamic nature of the sea-air interface distorted by water waves, two simultaneous pictures are necessary to obtain an instantaneous representation of the sea surface at one given instant. The first experiments with stereo cameras mounted on a ship were reported by Schumacher in 1939 (Gallego, Yezzi, Fedele, & Benetazzo, 2011). Stereography gained popularity in studying the dynamics of oceanographic phenomena during the 1980's due to advances in hardware. Lately advances in this field include analysis of sequences of images using CCD cameras, and improvements of analysis techniques, for accuracy and processing time.

Benetazzo (Benetazzo, 2006) for example described a technique for the measurement of short water waves from a sequence of synchronous, overlapping images recorded with two CCD cameras. They used the ideal pinhole camera model (Jähne, 1993) to describe the mathematical relationship between the coordinates of a point and its projection onto the image plane of a camera. This model, in which the camera aperture is described as a point and no lenses are used to focus light, does not take into account some effects linked to geometric distortions, blurring or discretisation of image coordinates. Most of these effects can however be compensated through a calibration procedure to result in a good description of how a camera depicts a 3D scene. The stereo camera model, in which three coordinate systems (one corresponding to the left camera, the other to the right camera and the last to the world or absolute coordinates) intervene, is shown here in Figure 21.

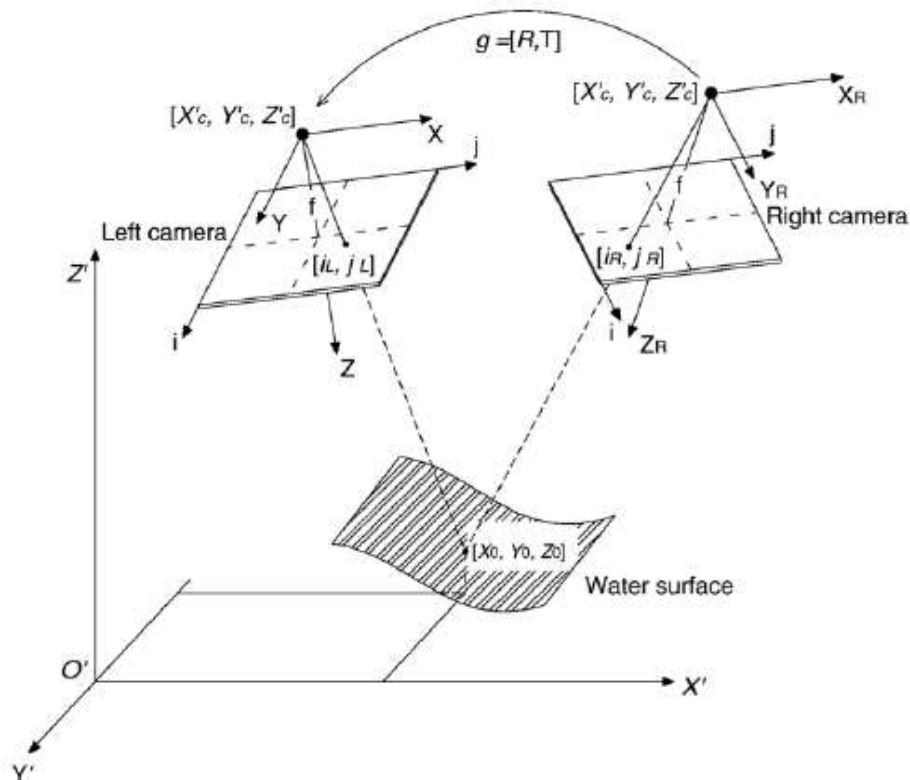


Figure 21: Stereo-camera model showing the setup of two camera stereometric intersection which allows determining the 3D coordinates of a point on the water surface. From (Benetazzo et al. 2006).

The main difficulty in stereo analysis resides solving the correspondence problem, i.e. in finding, given a point in the first image, the corresponding point in the second image. The stereo-processing presented in (Benetazzo, 2006) is based on a pyramidal pixel-based correlation method. It uses the principles of epipolar geometry (that defines a relationship between the camera image planes). They also use the hypothesis that the water surface can be locally approximated by a planar surface to reduce the search for corresponding points. Details of the algorithm can be found in (Benetazzo, 2006).

Since they acquired movies of the scene, the problem is a dynamic stereo reconstruction. The 3D location of corresponding points, obtained from the first couple of stereo-images, is exploited to reduce the region of epipolar search in the next frames, based on some preliminary evaluation of the wave characteristics. This reduction of the research range allows a reduction of computational time of about 80%. The comparisons they present of the free surface elevation obtained at a point with the stereo system with data recorded at the same point by an ultrasonic wave gauge show very good agreement.

Gallego et al. (Gallego, Yezzi, Fedele, & Benetazzo, 2011) identified two major disadvantages in using epipolar geometry. First, correspondences rely on strong textures, and image matching gives poor correspondences if the objects in the scene have a smooth radiance. Correspondences also suffer from the presence of noise and local minima. Secondly, each space point is reconstructed independently, and therefore, the recovered surface of an object is obtained as a collection of scattered 3-D points. Thus, the hypothesis of the continuity of the surface is not exploited in the reconstruction process, which is highlighted by holes in the reconstructed surface corresponding to unmatched regions.

They adapted modern image processing and computer vision methods, relying on calculus of variations and partial differential equations, to the reconstruction of the ocean surface. In their variational method, the reconstructed surface of the ocean is obtained as the minimizer of an energy function designed to fit the measurements of the ocean, therefore exploiting the continuity hypothesis in the full 2-D domain of the surface. After validating the numerical implementation of the proposed variational stereo method with synthetic data, they present results from experiments with real data.

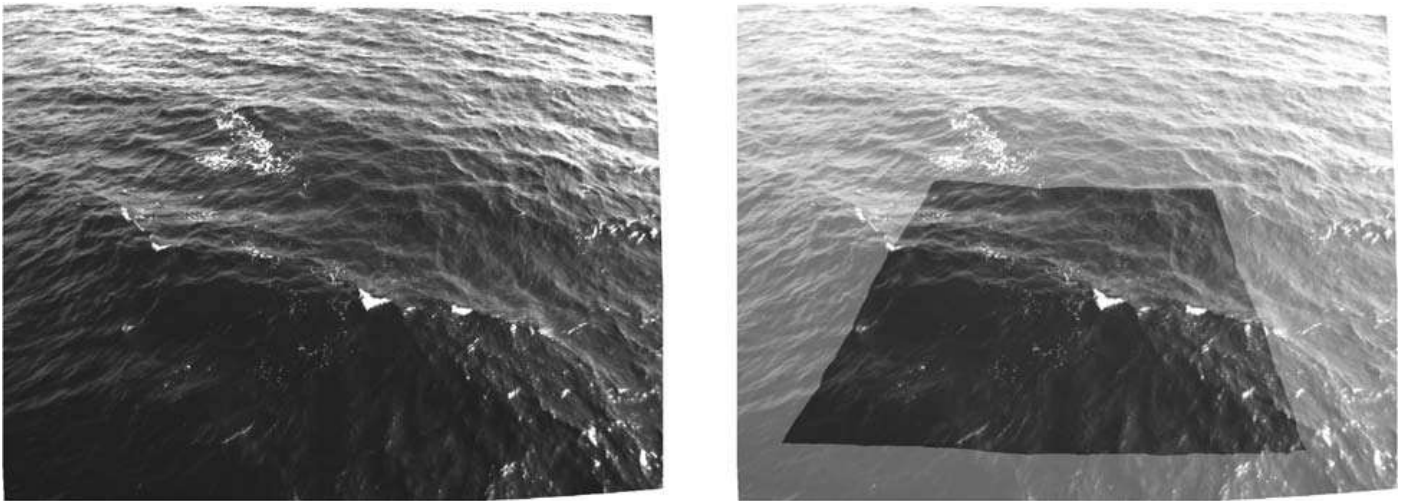


Figure 22: Original image of the sea surface taken during experiments in Crimea on the left and modelled image superimposed on the original on the right. From (Gallego, Yezzi, Fedele, & Benetazzo, 2011)

They used the 4D reconstructed wave surface to obtain spectra and statistics of the waves recorded. They then for example present the mean omnidirectional spectrum $S(k)$, averaged over 2000 snapshots, which clearly present a behaviour similar to that predicted by the wave turbulence theory of Zakharov [34], with the spectrum tail initially decaying as $k^{-2.5}$ up to small scales up to ~ 10 rad/m and then switching to a k^{-3} equilibrium range.

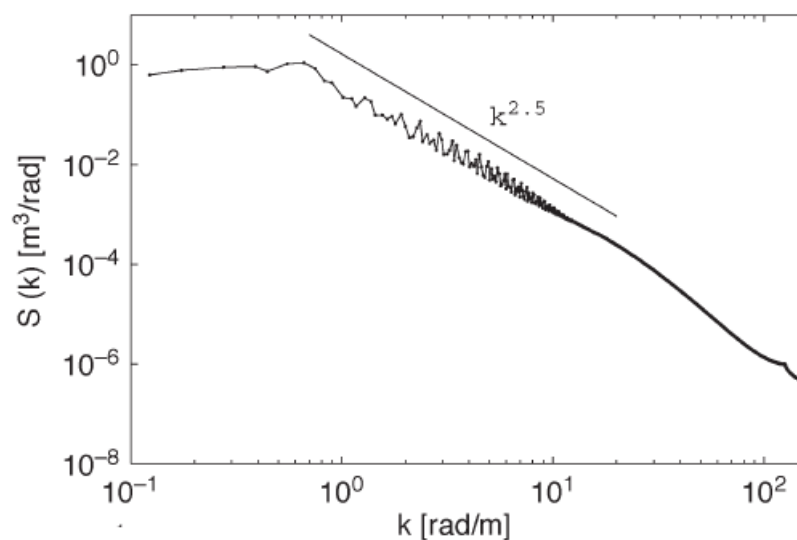


Figure 23: Mean omnidirectional spectrum $S(k)$ averaged over 2000 snapshots, from the Crimean experiments. From (Gallego, Yezzi, Fedele, & Benetazzo, 2011)

Fedele et al. (Fedele, et al., 2013) carried out further statistical analysis of the data recorded during the deployments of the WASS mentioned by Benetazzo and Gallego with the stereo technique described in Gallego. In an extreme value analysis, they showed that the maximum wave height over an area during a given duration (space–time extreme) is larger than that expected at a given point in space (time extreme). They demonstrated that space–time wave statistics can be obtained from stereo video imaging and that existing stochastic theories of wave extremes agree with measurements.

Bechle and Wu (Bechle & Wu, 2011) presented a method to obtain wave characteristics using stereo imaging less computationally-demanding than the point-cloud method. Their technique of Virtual Wave Gauge tracks the elevation of the water surface only at some selected points using an Eulerian based dynamic search algorithm. They

argue that this improves efficiency by two orders of magnitude compared to the traditional Lagrangian–Eulerian based point cloud method of stereo image processing. For their study, they used the trinocular ATSYS system.

ATSYS, developed by Wanek and Wu (Wanek & Wu, 2006), uses three cameras to address the issues of consistency and accuracy present in binocular stereo systems. It was successfully used to measure the temporal evolution of three-dimensional small-scale capillary waves and large-scale wave breaking. More details on ATSYS can be found in (Wanek & Wu, 2006).

2.4 LIDARS

Lidars are laser-based instruments measuring the distance to a target. A lidar sends bursts of laser light onto a target and detects through a photodiode the light reflected back from the target to the lidar. The phase difference between the signal sent and that received can be changed into distance using the time-of-flight principle. The term Lidar is commonly considered to be an acronym for Light Detection and Ranging, but it is also said to be a portmanteau of 'light' and 'radar' (wikipedia). Laser measurements are unaffected by the temperature of the water surface or by temperature gradients in the air between the sensor and the water surface, however they can be affected by water sprays and fog.

Scanning lidars use a mirror which rotates in one or two direction to obtain 2D profiles or 3D surfaces.

One of the first uses of a Lidar, named at the time a laser wave profilometer, for wave measurement was reported by Ross et al. in 1968 (Ross, Peloquin, & Sheil, 1968). The measurements obtained with the lidar mounted onto an offshore tower compared well with those made by a resistance wire wave staff situated close to the Lidar point of measurement.

Several investigators reported the successful use of lidar from aircrafts to spatially map the sea surface. Hwang et al. used a scanning lidar (Hwang, Wang, Walsh, Krabill, & Swift, 2000) placed on an aircraft flying at 500 m.

One experimental device using three laser altimeters to measure directional oceanic surface waves was tested in 2003 on the NOAA LongEZ aircraft (Sun, et al., 2005). The triangular array of laser altimeters was placed on the aircraft flying 15 m above the sea surface. The laser altimeters could measure between 5 and 50 m but the amount of dropouts in the data increased above 15 m, even if the 2 KHz sampling frequency of the altimeters provided redundant data that was averaged.

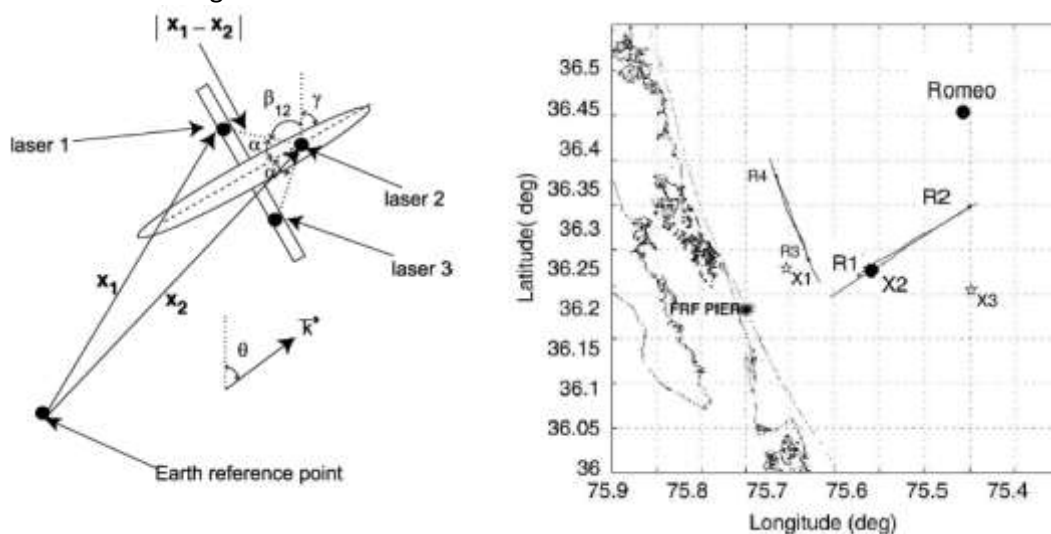


Figure 24: Schematic of the three laser altimeter array on the aircraft, and map the testing area with flight tracks (R1, R2, R3, R4), and positions of Datawell wave rider buoys (X1, X2, X3). Romeo is an ASIS (air-sea interaction spar) buoy. From (Sun, et al., 2005).

As illustrated by the flight tracks shown in Figure 24, the method, based on a wavelet analysis, requires the airplane to fly along a track with reverse headings, in order to resolve the wave propagation direction. The resolved wave number and wave propagation obtained during the 15 km-long flight track (R1,R2) did compare well with buoy observations at the site.

They showed that this technique can successfully resolve wave number and wave propagation direction, except under a number of singular conditions depending on aircraft and wave propagation speeds and direction.

Irish et al. reported the development and testing of a directional wave gauge composed of four lidars in 1999 at the U.S Field Research Facility in North Carolina (Irish, Wozencraft, & Giroud, 2006). The Laser Wave Gauge (LWG), placed on a pier at the US FRF, measured directional spectral wave characteristics from free surface measurements, above a PUV system placed below the surface for comparison.

The system presented next is, according to (Ardhuin, 2010), the only one able to provide directional spectra at a resolution better than that from buoy measurements.

Oil company ConocoPhillips Inc. installed on the Ekofisk oil platform in Norway the Ekofisk Laser array (LASAR) in February 2003. The LASAR array consists of four vertically looking Optech rangefinder lasers placed at the corners of a square with 2.6 m-long sides, 20 m above the surface and over a water depth of 70 m. The lasers determine the height of the sea surface below them by measuring the time from the emission of a light pulse to its detection after reflection at the air-water interface, with a 10^{-3} m accuracy. Krogstad et al. (Krogstad, et al., 2008) precise that with a continuous 5 Hz sampling the system provides directional spectra as well as a reliable surface tracking.



Figure 25: Picture of the Ekofisk oil platform showing the position of the LASAR array.

Luther et al. (Luther, et al., 2013), discussing validation and evaluation protocols of wave measurement systems, mention that the LASAR array was used as reference for verification and validation of wave buoys measurements in deep water (it is a deep water site for waves of periods lower than 14 s). They also report that the Datawell Waverider DWR-MKIII is the best available reference/standard for deep and intermediate water wave evaluations, as it was also extensively tested against measurements made at the 8 m-array (a 15-pressure probes array) at the US Field Research Facility. More details on the 8m-array can be found at:

<http://www.frf.usace.army.mil/8mArray/about8mArray.html>.

Latest advances in Lidar came with the recent introduction of flash Lidar cameras. These cameras, developed by Advanced Scientific Concepts Inc. (ASC), collect full frames of 3D point cloud data (up to 128 x128) per single laser pulse, up to 60 times a second (<http://www.advancedscientificconcepts.com/>).



Figure 26: Picture of the Tigerclub Flash Lidar camera.
From ASC' website

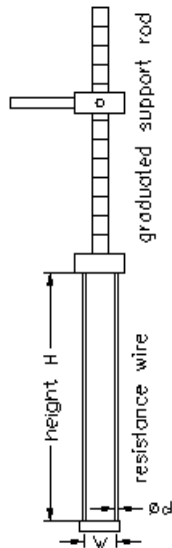
The images obtained can be straightforward interpreted as there is no distortion problems linked to camera lenses as with stereoscopic vision. Because all data points are taken simultaneously, the motion of the platform does not affect the measurements, as is the case with scanning lidars. These systems are also light (under a kilogram) and compact in size (around 10 cm x 10 cm x 10 cm).

The authors of the present report are not aware at the time of writing of this system having been tested to measure the surface of an air-water interface. ASC mentioned in a private communication that the system is still under development for measurement of air-water interface. However, Grilli et al. anticipated developments in this technology and reported on the development and validation of free surface reconstruction algorithms to predict ocean waves, based on spatial observations that would be made with a high frequency Flash LIDAR camera (Grilli, Guerin, & Goldstein, 2011). The camera considered generates a 64 x 64 matrix of laser rays, providing as many simultaneous measurements of the distance to the ocean surface, every 0.05-0.25 s, in an angular sector of 15-20 by 9-15 deg. In this paper, the authors did not use actual experimental data set from a Flash Lidar camera. They simulated dynamic ocean surfaces, and data point clouds that would be obtained from a flash Lidar camera. They tested and validated free surface reconstruction algorithms based on a linear or 2nd-order representation of 1D and 2D irregular ocean surfaces, whose parameters are estimated based on minimizing the mean-square error of simulated surface elevations to measurements, over space and time (for a specified time prediction window). Once sea state is properly estimated, a prediction of expected waves ahead of the vessel can be made; the process is then repeated for another prediction window, and so forth. In the case of a 2D linear reconstruction using spatio-temporal data, they show that a short term forecast of the ocean surface in a fairly wide strip in the main aiming direction of the camera can be accurately and efficiently generated.

Such short-term forecasting of ocean waves could be much beneficial to wave energy converters, for example possibly allowing adjustment of the damping level of the WEC in order to optimise wave energy extraction, or to lower structural loads.

3 NON-INTRUSIVE WAVE FIELD MEASUREMENT IN WAVE TANKS

The most common instrument for wave measurement used in hydrodynamics laboratories are resistance type gauges, consisting typically of two thin, parallel vertical metal rods partly immersed, as shown in Figure 27.



The water height is derived from the conductivity between the rods which increases with the immersion of the rods. They usually are reliable and robust. Moreover, they can easily be manufactured in-house at low costs. For a good accuracy, they have to be calibrated for the largest waves to be measured in a test campaign. Their calibration is however not very stable and has to be repeated regularly (in [x] it is suggested twice a day). A meniscus tends to form on the rods at the air-water interface, leading to measurement errors which can be significant when measuring small waves [x]. Large measurement errors can also occur if the wave gauge is moving with respect to the water surface: this situation would typically occur in a towing carriage or if a water current is present in addition to waves.

The thermal stratification of the water can affect their measurements.

Figure 27: scheme of a resistive wave probe.

The hydrodynamic loads on them can become large for example when used to measure high amplitude waves, or when towed at high speed, for example from the carriage of a towing tank.

Capacitance wave gauges are usually preferred in this case, as they are less intrusive since they can be reduced to a single thin wire. They also allow measurement of the wave elevation in a point over a larger range of amplitude. Other usual instrumentation used in laboratories comprises mechanical profile followers or pressure sensors in combination with velocity sensors.

3.1 OPTICAL SENSORS

Optical wave gauges in contrast tend to be non intrusive. They rely on imaging and identifying features on the water surface that can be tracked or correlated in time and space. The water surface is a specular reflector and at tank scale it lacks naturally occurring features that could provide texture elements recognisable by an image analysis system, so optical wave height measurement techniques rely in general on structured lighting of some sort to create the required features at the water surface.

In most cases the structured lighting is provided by a Laser source. Compact solid-state Laser sources (DPSS modules) have been available cheaply for some time and there is plentiful choice thanks to accelerating advances in laser diode technology and to massive proliferation of manufacturers worldwide, particularly in Asia.

In the last decade the advent of affordable, high quality CCD and CMOS camera sensors on one hand has spawned a host of research projects and developments in optical measurement systems. Even machine vision cameras mass-produced for industrial applications such as automated quality control, dimensional or integrity checks, have functionalities and a level of image quality that makes them suitable for a whole spectrum of quantitative measurements of dynamic phenomena in science and engineering: tracking, ranging, profilometry, motion and deformation analysis to cite but a few.

3.1.1 Optical triangulation wave probe

This section presents the development of a point wave height measurement technique based on optical triangulation and using a laser pointing at the water surface. Part of this work was reported in (Payne, Richon, Ingram, & Spinneken, 2009).

Working principle

A Laser source is located above the water surface and beams vertically downwards, generating a spot of scattered light at the water surface and a line of scattered light below the water surface. The spot and the line are imaged by a digital camera with an off-axis line of sight and a fixed position relative to the laser source. The up- per end of the line of scattered light and the spot correspond to the water surface. Their precise location on the camera images are derived by image processing and transformed into a height value using a polynomial best- fit function established by an initial calibration. This principle is illustrated in Figure 28 where two side view sketches show the water elevation measurement technique at a wave trough (Figure 28(a)) and at a wave crest (Figure 28(b)). The right hand side part of each sketch represents the image seen by the camera. The position of the spot is at the lower end of the range for the wave trough (Figure 28(a)) and at the upper end for the wave crest (Figure 28(b)).

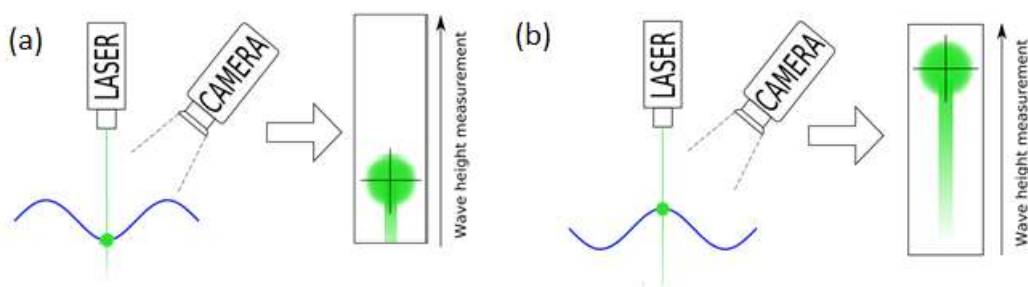


Figure 28: Principle of functioning of the optical triangulation wave probe.

An optical wave gauge based on the same principle was developed in the early 80s (Liu, Katsaros, & Weissman, 1982). A line array of 256 photodiodes was used instead of the camera. This gauge was used to study capillary waves with amplitudes of the order of 10 mm.

The system examined here has a nominal range of 300 mm and uses a standard Charge-Coupled Device (CCD) camera with a VGA resolution (640×480 pixels). The range can be modified by the use of different camera lenses. Lenses with longer focal lengths will provide a shorter range but a finer resolution whereas lenses with shorter focal lengths will yield an increased range but at the expense of resolution. The laser used is a 200 mW Diode Pumped Solid State (DPSS) Laser with a 532 nm wavelength. The calibration of this gauge is very stable in time as it only depends on the geometric parameters of the gauge set up. On the other hand, external factors such as lighting and water surface quality must be minimised, as discussed in the next section.

Calibration is achieved by translating vertically the laser-camera assembly above still water over a height corresponding to the range of the gauge. Images are acquired from the camera for a set of known vertical positions. Those images are used in combination with the height value at which they have been taken to derive the calibration curve of the gauge.

Image acquisition and processing

The image acquisition and processing sequences must ensure a reliable and accurate detection of the laser spot on the free surface. On the recorded images the spot is always followed by a ‘tail’ of scattered light extending far below the water surface. The general principle underlying the detection of the spot and tail signals relies on statistical

analysis of the grey-level pixel intensities along one or both axes of each image. An example image and the corresponding grey-level intensity profile are given in Figure 29.

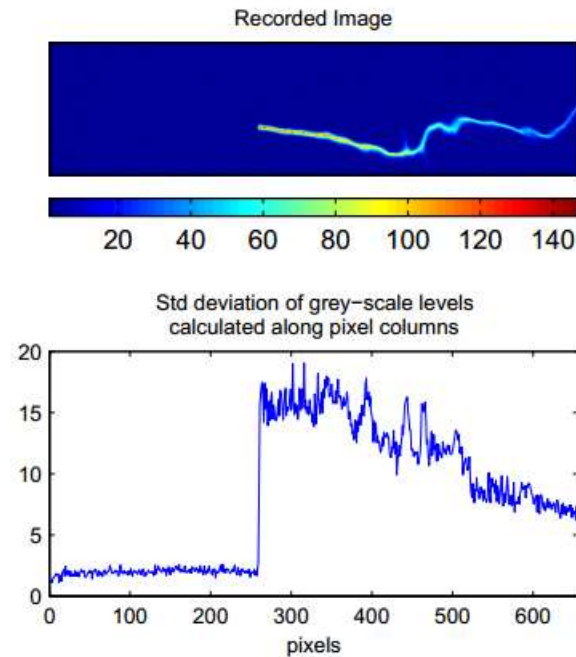


Figure 29: Example of image recorded and corresponding grey-level intensity.

At the water surface, the appearance of the spot as seen by the camera will vary significantly with local wave slope, reflections caused by ambient lighting and contaminants that may be present at the point of impact of the beam, for instance solid particles or hydraulic oil. Probe settings are therefore adjusted so as to minimise any effects that these external factors may introduce in the measurements. The impact of ambient lighting can be largely removed by using a bandpass filter with a 532 nm centre wavelength, and by sampling only a narrow strip of image centred on the path followed by the laser beam on the images during the measurements. To further reduce the impact of variations in the optical quality of the water surface on detection, the image exposure time is set to the shortest time still providing sufficient contrast in the image between the laser beam path in the water and the dark background. The use of the shortest possible exposure time is also essential to minimise any time-averaging effects due to water motion occurring while the image is being recorded.

Two alternative image processing approaches were implemented to detect the laser beam impact point on the water surface: one based on centroiding the spot image, the other based on grey-level threshold detection. Centroiding techniques offer a potential performance advantage over thresholding techniques since they inherently resolve the spot position to sub-pixel accuracy. In practice however, the spot shape and intensity profile were found to vary greatly in time; furthermore, in many cases the image of the beam intersection with the water surface looked much closer to a thick line with barely or no distinguishable spot feature at its extremity. In these cases, centroid detection actually tended to yield poorer results than threshold detection. Overall it was found that thresholding algorithms could be made to perform more consistently and over a broader range of operating conditions than their centroiding counterparts.

Calibration rig



Figure 30: Picture of the calibration rig used for the optical wave probe.

The calibration rig is designed to be an integral part of the optical gauge itself. It can translate vertically the Laser-camera assembly over a 300 *mm* range. A picture of the rig is shown in Figure 30.

The Laser and the camera are mounted on a ‘translating beam’ which is itself fastened to the moving block of a linear guide. The ‘moving assembly’ is driven up and down by a linear actuator. The actuator is fitted with a coarse digital motion encoder which allows position control with an accuracy of the order of 1*mm*. To get more accurate height values, the rig is fitted with a digital scale unit whose absolute precision is 40 μm . The way the system is used for calibration is as follows. A target height is chosen. It is assigned to the control system of the linear actuator which relies on the optical wave gauge with that of a conductivity wave gauge in regular wave.

Validation of the Technique

The tests were done in the University of Edinburgh curved tank. A resistive wave gauge was placed for validation of results 210 *mm* away from the laser probe, in order to minimise the effect of ripples radiated from the resistive wave probe on the laser wave gauge, the line between the conductivity gauge and the laser beam being parallel to the incoming two-dimensional wave fronts.

Figure 31 shows the time series for both wave amplitudes investigated. The signal from both gauges is compared with a fifth order Stokes theoretical solution. Given the relatively deep water conditions (water depth of 1.2m for 1Hz waves) and the moderate steepness of the waves considered herein, this solution is regarded as an adequate reference. Deviation of the measured data from the theoretical solution is therefore considered to be due either to measurement inaccuracies or to spurious tank cross waves. It should be noted that the phase and height of the Stokes solution were adjusted to fit those of the gauge signals.

The measurements from the optical wave gauge matched very well the theoretical solution for the 25 *mm* amplitude waves (corresponding to a wave steepness of 0.1) whereas some small deviations, in particular at the wave crest, remain when using the conductivity wave gauge. The discrepancies between the two measurement techniques are substantially more pronounced when considering steeper waves (amplitude of 50 *mm*, corresponding to a steepness of 0.2). Whilst the accuracy of both gauges is comparable in the vicinity of the troughs, the optical wave gauge yields a reading closer to theory at wave crests. The bottom plot of both figures shows that the optical wave gauge accounts better for the higher order wave components than the conductivity gauge.

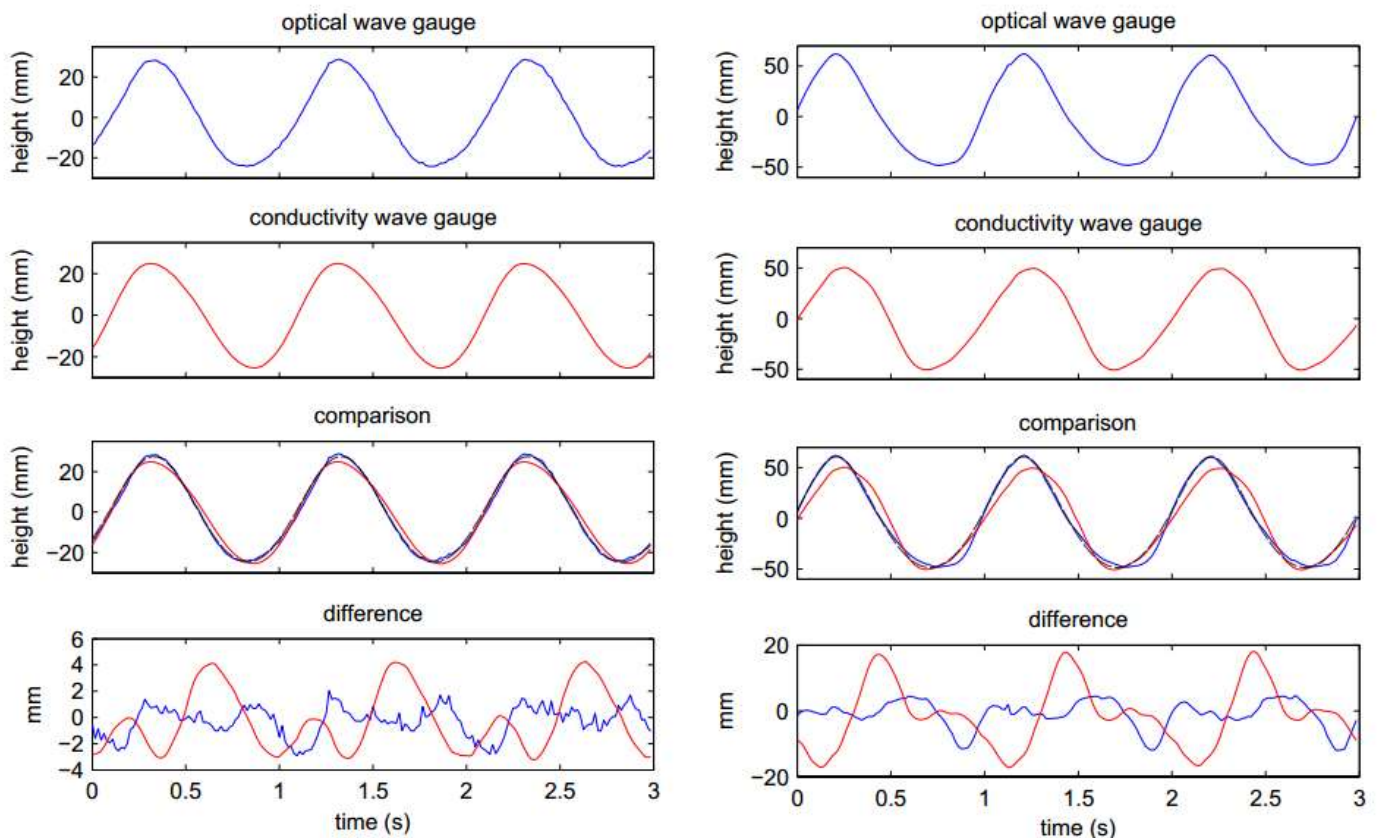


Figure 31: Wave elevation time series for the optical (blue) and conductivity (red) wave probes. On the left for 25 mm amplitude waves, for 50 mm amplitude waves on the right. The third plots compare the measurements with 5th order Stokes theory, while the fourth plots show the respective differences with Stokes theory.

The optical triangulation probe is sensitive to several parasitic effects that degrade its performance:

- False positive readouts caused by dust particles crossing the laser beam on the air side
- Changes in time of the water turbidity causing large variations in scattering efficiency of the water surface
- Changes in time of the surface scattering properties due to contamination of the water surface (e.g. by oily films)

Most of these effects can be mitigated or eliminated by careful design of the image processing algorithms and by introducing a degree of adaptive behaviour in the image acquisition process.

Overall this technique is very suitable for small scale wave tank testing and represents a viable alternative to standard intrusive wave probes when water or probe motion is present.

3.1.2 Laser slope gauges

Another technique relying on lasers to characterise wave fields was presented for example by Sanker and Shemer (Sanker & Shemer, 2012). It consists in measuring wave slope by exploiting the difference in refraction index between air and water. A Laser source is located below the water surface and is beaming vertically upwards. As the beam reaches the air-water interface, it is deflected from vertical according to Snell's law. The deflection angle is a function of the water surface angle to the vertical and of the ratio of the water refraction index to that of air. The deflected beam is collected above the water surface by an aspheric lens which focuses it on a photo detector. The lens is designed in such a way that the distance of the resulting laser spot on the photo-detector plan to the optical axis is proportional to the beam angle of incidence onto the lens. This technique does not actually measure wave height but wave slope, in two directions. According to their authors, the technique lead to good results for slopes up to 44 degrees, and with high-frequency waves (>50 Hz).

It is mainly used for spectral analysis of small waves such as capillary waves. Although this system does not directly interfere with the water surface where the slope is measured, it still can be considered as intrusive in that it requires the laser source to be located at some depth below the water surface. However the laser source can be considered non-intrusive if its presence does not affect the wave field, which depends on the water depth and wave length.

3.1.3 Lidars

Because lidar is effectively a time-of-flight measurement where light is the information carrier, its accuracy degrades sharply when the stand-off distance between the probe and the water surface is reduced to values compatible with a laboratory wave tank, i.e. less than 10 m, typically a few meters. With recent developments in high-speed data acquisition, gating temporal resolutions in the picosecond range are now achievable for time-of-flight measurements. This suggests that LIDAR techniques now have the potential to be applied to wave height measurements in a wave tank environment.

Blenkinsopp (Blenkinsopp, Turner, Allis, Peirson, & Garden, 2012) studied the propagation and shoaling of waves using a LMS200-30106 scanning lidar manufactured by SICK along a 6 m-long test section within a laboratory wave flume. The LiDAR was mounted 3.55 m above the flume bed centreline, 6.75 m upstream of the slope crest and orientated to scan along the length of the flume.

They mention that detection of water surfaces using a laser measurement system can be problematic because reflections from a smooth water surface are specular and so a return is only achieved when the incident angle of the laser is approximately perpendicular to the surface. They added some kaolinite, a clay mineral with a particle size (D_{50}) of 20 μm , to the fluid. The presence of particles greatly increased the number of signal returns obtained from a flat water surface and valid free-surface measurements were obtained over the full test region for laser beam angles (taken from the vertical down) between -39.5° and 75° . They mention that for their experimental setup, the limiting angle between the lidar beam and wave face (interpreted as the normal to the wave surface at the measurement point) was 28.5° . The response of the lidar is affected by the location of the instrument relative to the main area of interest and as such, careful consideration should be given to instrument positioning and initial verification of instrument accuracy should be carried out on a case-by-case basis.

The comparison presented between lidar measurements and those from capacitance wave probes show very good agreement, with differences equivalent to a maximum of 2% of the wave height measured, which is of about the same order of magnitude as the estimated capacitance wave probes' accuracy.

They conclude by noting that their results provide encouraging evidence that for applications where detailed measurements of wave profile are required, a single lidar instrument can replace large arrays of conventional wave probes and provide much higher spatial resolution than can be practically achieved using conventional laboratory instrumentation.

A similar Lidar was used at Leibniz Universität Hannover (LUH) in a study involving several combined measurements, related in section 3.5.

3.2 ACOUSTIC SENSORS

3.2.1 Ultrasonic sensors

Ultrasonic sensors used in wave tanks are similar to those used at sea presented in section 2.1.2. Such instruments are placed usually at around a meter above the water surface, looking vertically downwards. They are easy to use as they only need the distance separating them from still water level for calibration.

MASSA M300/95 ultrasonic sensors were for example used by Vousdoukas et al. at the FZK to obtain data to validate 2D laser scanner measurements (Vousdoukas, et al., 2014). (see section 3.5). These sensors have a range between 10 cm and 4 m, they have built-in temperature compensation for sound speed, and can be programmed to have a large sensitivity over a given range.

3.3 RADARS

The use of marine radar in wave tank is quite uncommon, however Hofland et al. tested a RADAC radar in the Deltares delta flume (Hofland, Hoffmann, & Lindenberg, 2012). This flume is quite exceptionally large, measuring 240 m in length, a width of 5 m and a depth of 7 m. As shown by Figure 32, they observed that spikes, or missing data points, can appear in measurements obtained from the radar for steep waves.

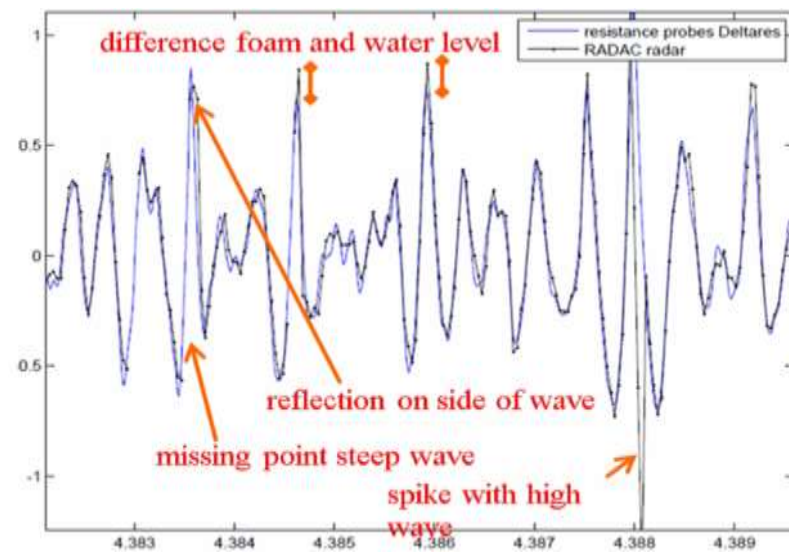


Figure 32: Comparison between measurements from a resistive wave gauge and radar in the Deltares delta flume, for a wave condition with large steepness ($H_{m0}=1.3m$, $T_p=5s$). From (Hofland, Hoffmann, & Lindenberg, 2012)

Small differences between the measurements can also be due to small differences in wave height over the crest of the wave (the radar measured in the centre of the flume and the wire gauge at the wall). At the highest wave crests the wire gauge tends to measure the solid or “green” water, while the radar tends to measure the uppermost (foam) surface. With the spikes are filtered out, they obtained percentage differences for significant wave height and mean period.

RADAC radars, having a 10 Hz sampling rate, were then installed in the delta flume as they are very flexible to use since they do not need any calibration.

3.4 IMAGING METHODS

One of the most straightforward imaging methods to obtain information about the wave field in a two-dimensional wave tanks is to look through a glass side-wall of the tank to record a free surface profile using a camera and thresholding operation and edge detection algorithms. However, while viewing the flow field from the side, the water interface surface is obscured by sidewall effects such as the presence of a meniscus and boundary effects. Such method of looking through a glass side-wall is also mainly used to study two-dimensional wave fields, as generated in narrow wave or towing tanks and it would not be applicable in large-scale wave tanks where glass side walls are not present, and where the flow (and its free surface) is fully three-dimensional.

Other imaging techniques have been developed for two-dimensional measurements of water waves in a large wave tank.

3.4.1 Laser sheet-based technique for free surface measurement

Perelman et al. describe in (Perelman, Wu, Boucheron, & Fréchu, 2011) a laser sheet-based system to measure the wave elevation along a line in a towing tank. As shown in Figure 33, a laser sheet is projected upwards from the bottom of the tank. A series of five cameras were installed to record the position of the intersection line between the laser sheet and the free-surface.

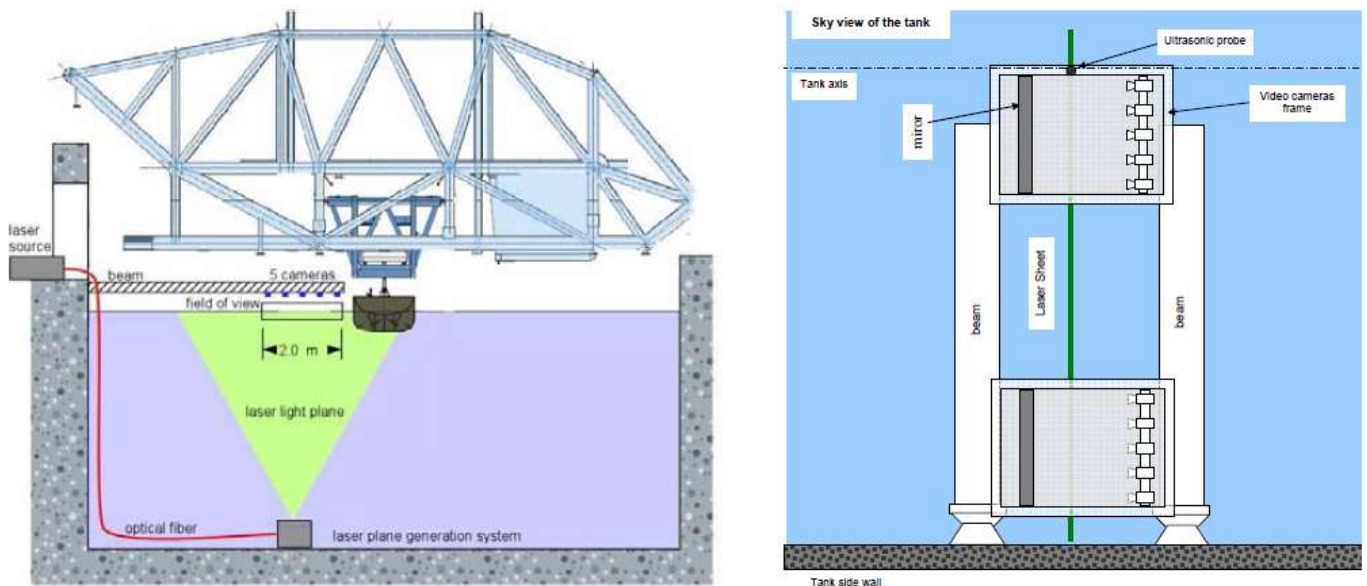


Figure 33: Description of the experimental setup used by (Perelman, Wu, Boucheron, & Fréchu, 2011). From (Perelman, Wu, Boucheron, & Fréchu, 2011)

Measurement of the free surface elevation was therefore obtained over a line, of 2 m length. This system needs to be calibrated to relate the water surface elevation to the displacement of identified pixels on the cameras. Only some light image processing is required to obtain the free surface elevation. They report the use of floating particles to sharpen the contrast of the intersection line seen by the cameras. This technique yielded good results with non-breaking waves. The scattering of the laser light in a breaking wave, due to the high concentration of bubbles and drops, renders that part of the domain unusable.

As the towed model passes by the laser sheet, 3D maps of the wake of the model could be obtained. The comparison between the free surface elevation measured at a point with this system and that obtained at the same point with an ultrasonic wave probe showed good agreement. They mention that this technique is mature, but that the setup is not easy to install in a tank.

3.4.2 Particle Image velocimetry

Particle image velocimetry (PIV) is a well-established technique allowing the measurement of the velocity of particles suspended in a fluid, in a plane illuminated by a laser sheet, as illustrated by Figure 34.

The particles used have usually a density very close to that of the fluid and are very small, so that they follow the fluid carrying them. A sequence of pictures taken with high frequency cameras is then used to obtain instantaneous measurements of fluid velocities. PIV is generally a difficult technique to setup in a wave tank, necessitating at least one high-speed camera, seeding particles and good lightning conditions. It is nevertheless still used in some cases, as it results in a rich description of the flow dynamics, usually over a two-dimensional plane.

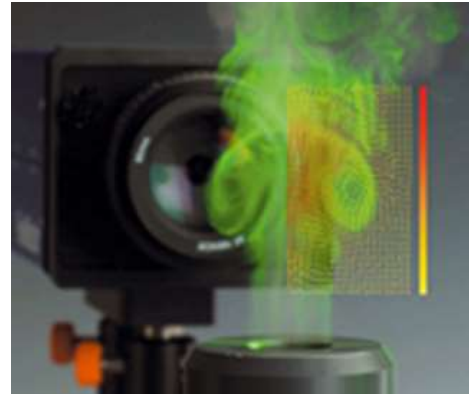


Figure 34: Illustration of principles of PIV. From <http://www.lavision.de/en/products/flowmaster/>

PIV is usually employed to investigate turbulence in a flow. It is a difficult technique to use to study wave-structure interactions, as for MRE research, primarily due to the motion of a body in the investigation area. It can however be used to study some specific fluid-structure interaction problem, usually in simplified cases. Osterried (Osterried, 2010) for example reported the study of the wave-structure interaction around an Oscillating Wave Surge Converter using PIV measurements. The velocity maps obtained during regular waves, shown here in Figure 35, allowed investigating the fluid-structure interaction, using also PIV-derived pressure measurements.

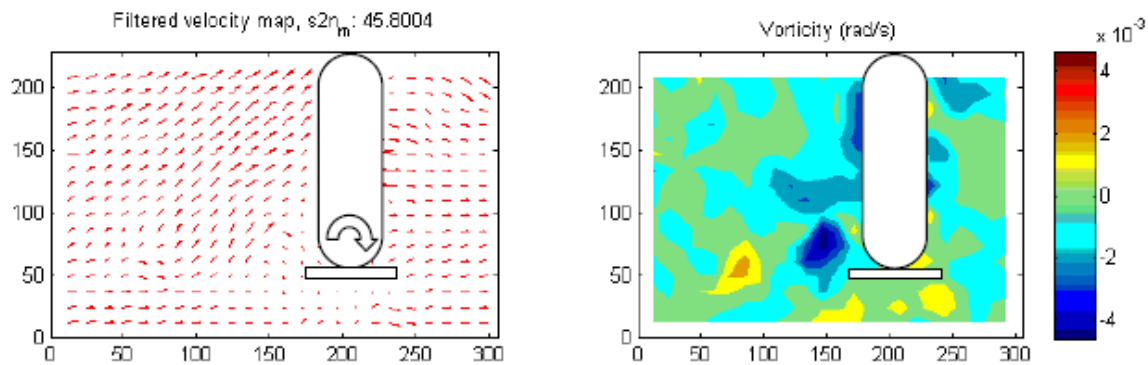


Figure 35: Velocity and vorticity maps around an oscillating wave surge converter. From (Osterried, 2010).

Other aspect of MRE are extremely related to turbulence flows, e.g. in the wake behind a tidal turbine. Good knowledge of the wake generated by a tidal turbine in its environment is for example necessary to estimate the appropriate spacing of tidal devices in a farm. Good et al. (Good, Hamill, Whittaker, & Robinson, 2011) used a 2-component PIV system to measure the velocity profile within the near-wake of a scale model of the four bladed rotor of the prototype 'Evopod' device, designed by Ocean Flow Energy. (www.oceanflowenergy.com). They mainly used their measurements for validation of a CFD model of the turbine, later to be used to simulate the wake of larger devices.

It can be noted that several extensions of the classical PIV system have been proposed to achieve more than two-dimensional, two component velocity information, as related in (Liberzon, Gurka, & Hetsroni, 2004). The most common extension is stereo-PIV where a second CCD camera is used to acquire the stereoscopic view of the flow, and obtain the out-of-plane component of the velocity on a plane.

Some systems can achieve three velocity components in a volume (3D3C) using two or more cameras. Holographic PIV, using volume illumination and complex holographic recording procedures, can provide an instantaneous three-

dimensional field with high spatial resolution, but it is for the moment limited to relatively simple flow configurations.

3.4.3 Stereo-Imaging

Stereo imaging has been attempted in laboratories with different levels of success. If the principle remains the same as for stereo imaging at sea, the difficulty here resides in obtaining images with high enough contrast. Waves in a wave tank present a smooth glassy surface. Pictures of such waves usually present one or more halo of light, and perturbations from the tank floor due to water transparency and/or from reflections. Perelman et al. (Perelman, Wu, Boucheron, & Fréchet, 2011) show typical pictures of waves taken at sea and in a wave tank, reproduced here in Figure 36. The difference in contrast in both images is clearly visible, and illustrated by the difference in distributions of grey levels also shown in Figure 36.

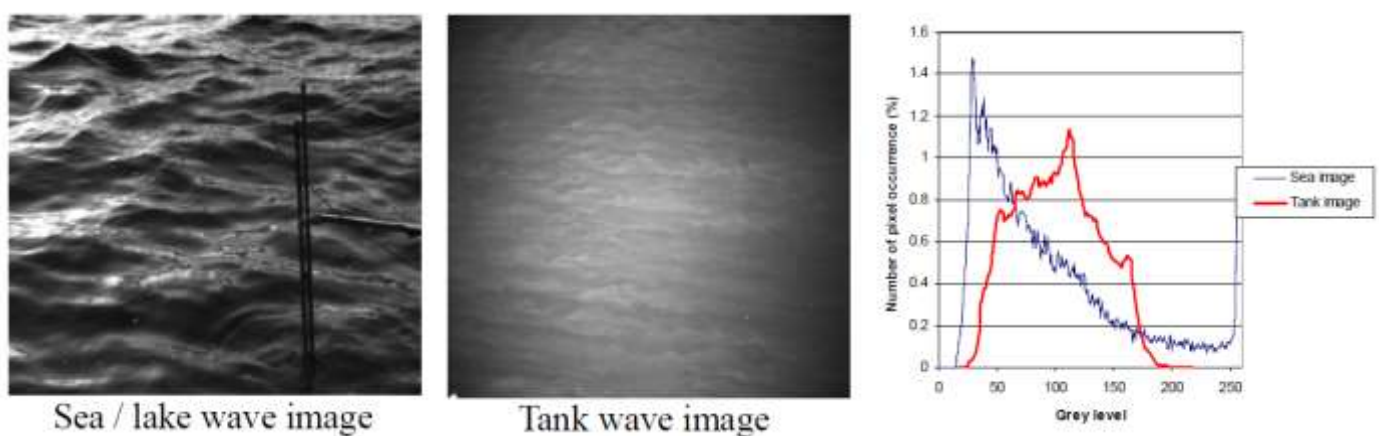


Figure 36: Differences in quality of typical pictures of waves taken at sea and in a wave tank. From (Perelman, Wu, Boucheron, & Fréchet, 2011)

Because of the low contrast in the pictures usually taken in a wave basin, the matching algorithm needed to solve the correspondence problem does not provide good results, yielding no possible stereo analysis of the recorded waves.

Perelman et al. attempted to roughen the free surface to get higher contrast by blowing wind on the water to superimpose capillary waves to the longer waves to be recorded, but still obtained poor matching results. They then seeded the free surface with floating particles (Chemigum particles of density 1.01 with median sizes of $600 \mu\text{m}$), using a fan. This seeding of particles, accompanied with a careful lighting of the free surface, resulted in the success of the stereo matching algorithm. 3D reconstructions of the free surface were then obtained, from which they could extract the wave elevation in a point, shown to be in good agreement with ultrasonic measurements done at the same point. It has to be noted that the seeding technique presented some limitations. After a while the particles were agglomerating in small packets, resulting in inhomogeneous distributions. The seeding particles were also a source of pollution of the surface.

Piepmeier and Waters (Piepmeier & Waters, 2004) managed to reconstruct the free surface of water waves in the 300 ft (91.3 m) wave tank at the Davidson Lab at the Stevens Institute of Technology by texturing the water surface with a fine mist, reducing problems of reflection and transparency. They studied an area of about $0.5 \text{ m} \times 3.5 \text{ m}$ with a commercial stereo vision system from Point Grey research. For tests carried out with monochromatic waves, the wave heights obtained were up to 9% lower than those measured by resistive wave probes. They argued this could be due to a dampening effect of spraying the water.

3.5 COMBINED LASER-SCANNER AND VIDEO HYBRID SYSTEM

3.5.1 Introduction

Among all the WECs, Overtopping WECs (OWECs) are one of the most promising technologies. The working principle of OWECs is based on waves running up a slope and overtopping into a reservoir. There is a recent interest towards the implementation of WECs units into near-shore sea defence structures, such as breakwaters. Such a concept tends to be more economically viable compared to single offshore floating WEC units. Regarding the efficiency of these WECs, it was demonstrated that the geometry of a near-shore OWEC, i.e. its ramp slope, plays a very important role on the amount of wave energy that is captured, Victor et al., (2011); this means that if the geometry of the device is adapted in terms of the incoming wave fields, the power output is increased. Thus, during the optimization process by means of physical experiments it is very important to further characterize the incoming wave fields close to the device, e.g. to monitor wave run-up over the swash zone.

As above mentioned, physical model tests are a fundamental part in the development of an OWEC, hence the importance of developing accurate techniques to measure wave fields at the swash zone. The techniques to perform precise and reliable measurements of the environment by avoiding contact with the measuring domain are called non-intrusive; among other advantages, their effect on the environment tends to be minimum or negligible, therefore the laboratory effects are minimized.

The Coastal Research Center 'Forschungszentrum Kueste' (FZK), member of Leibniz Universität Hannover (LUH) focused on the development of a non-intrusive methodology to measure water wave conditions in the vicinity of a ramp. Therefore, a new hybrid system consisting of a combination of laser scanners and video cameras was developed to monitor the wave run-up on a wave-by-wave basis. The methodology was implemented during large-scale experiments with a linear slope, the experiments took place in the Large Wave Flume (Großer Wellenkanal, GWK) of FZK. The experimental set-up is shown in Figure 37.

3.5.2 Materials and methods

3.5.2.1 Hardware and synchronization

The system developed is composed of different measuring devices, see Figure 37. Calibration of each component was needed in order to gather measurements synchronized both in space and time. The water elevation along the swash zone was measured at 8 Hz by a 2D laser scanner SICK LMS291. The angular range of the 2D scanner was 90°, whereas the radial range varied from 10 m to 30 m. The 2D scanner was governed by the software RACK (Robotics Application Construction Kit).

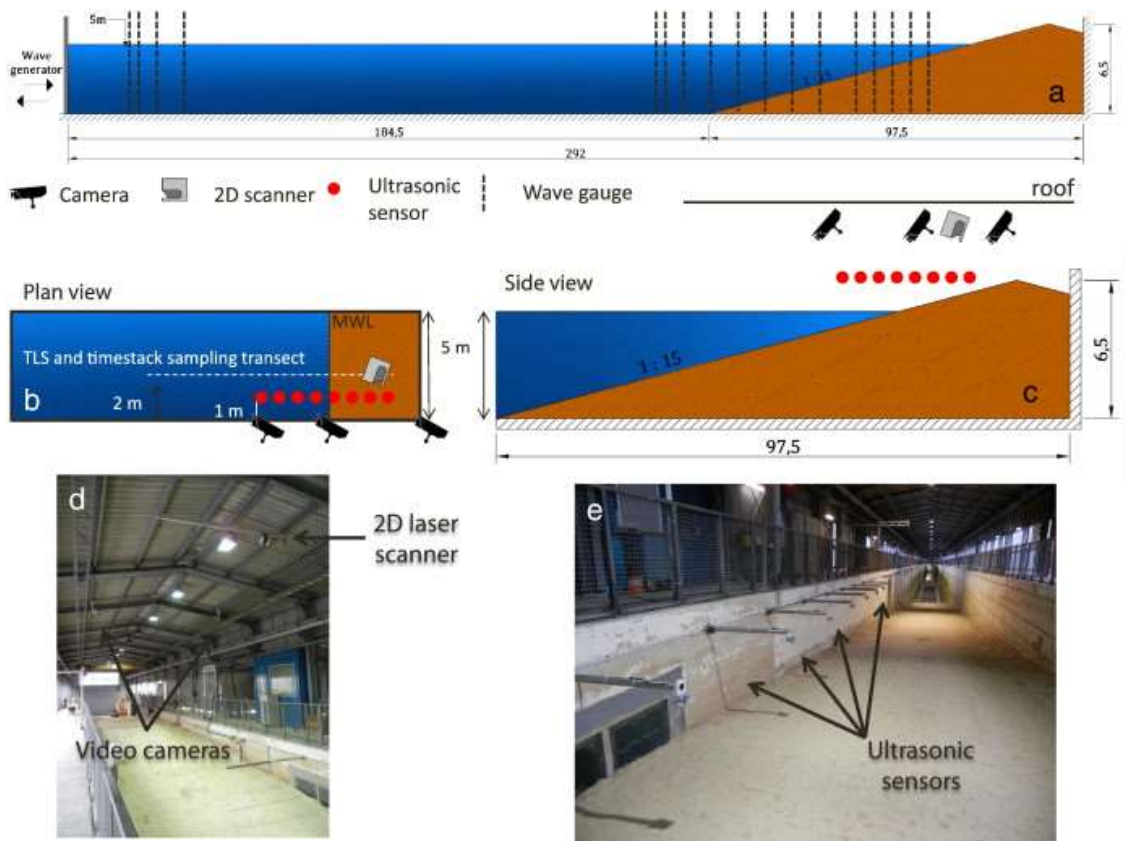


Figure 37: Side view of the flume showing the wave gauge positions (a), as well as side (b) and plan (c) views indicating the locations of the video cameras, the laser scanner and the ultrasonic sensors. The cameras as well as the ultrasonic sensors are also shown in pictures (d, e). *From Vousdoukas et al., (2014)*

The swash zone was also monitored by means of three cameras, AVT MANTA G-125, 1.3 MP cameras, Fig.1. Imagery along the swash zone was recorded at 5 Hz, the cameras were controlled by a GS-Vitec Marathon Pro software, the synchronization was conducted by a central data acquisition system. For the sake of minimizing the geo-location errors due to small grazing angles the cameras as well as the 2D scanner were located at 12 m over the mean water level.

3D digital elevation models of the experimental set-up with an accuracy below 0.5 cm were provided by means of a FARO 3D scanner, based on the phase shift principle. High resolution data about the locations of the instruments whereas the ground control points was extracted from the digital elevation models. During the calibration and data processing, the combination of the different measurements provided by the different measuring devices allowed increasing the quality of the recorded data. The final output is a continuous measurement of the free surface elevation at the swash zone in 2D-space and time, see Figure 38.

3.5.2.2 Calibration of the 2D scanner

The 2D scanner has to be deployed in order to ensure that the measurements are along a vertical plane, parallel to the x axis. All the recorded measurements have to be translated (along x and z) and rotated (along y axis) in order to be converted to the global coordinate system. The mentioned process was developed by taking into account the ground control points placed along the scanner's measuring plane. In order to avoid the distortion of shapes by the 2D scanner, this was additionally calibrated by scanning water, dry slope and concrete surfaces from an equal distance respect to the experimental set-up, therefore the shape distortion was evaluated. In this sense, empirical coefficients were used to process the data.

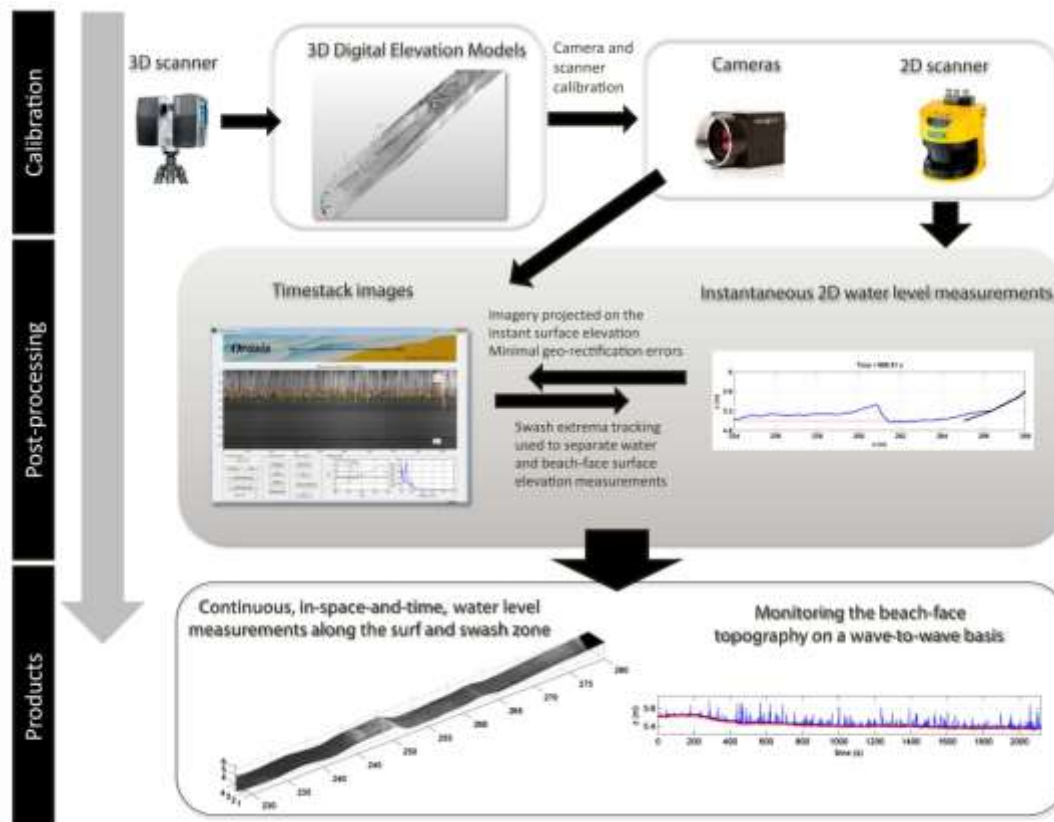


Figure 38: Main components of the laser scanner-video hybrid system. From Vousdoukas et al., (2014).

3.5.2.3 Image geo-rectification

Standard photogrammetric procedures, e.g. lens-distortion compensation, were employed to transform the images to GWK coordinates. This process is known as image geo-rectification.

3.5.2.4 Measuring wave run-up

By sampling pixel intensities over the 2D scanner recording area, images were acquired and used to create timestack images. In order to reduce artefacts given by monoscopic view, the timestacks were created by considering the horizontal area of the zone to be monitored whereas the instant free surface elevation measured by the 2D scanner. The timestack images were used to provide time series of the cross-shore position of the swash events.

In order to monitor the swash and surf zone water surface elevation, continuous elevation measurements over the monitoring area were gathered by the 2D scanner, whereas pixel intensity information was provided by the video images. A typical problem when measuring wave run-up is to separate the water from the solid parts, therefore a certain methodology has to be applied to reduce the uncertainties. The method is explained as follows, an easier separation of the submerged and dry parts of the slope is allowed by the timestack image processing, which provides the swash edge position. Once the separation is conducted, the swash whereas an important part of the surf zone can be monitored by the hybrid system and measurements of the free surface elevation along the swash zone can be taken. These are the main steps of the process:

- The wave run-up time series were used to identify the time intervals between consecutive swash events, therefore each event was individually processed.

- The immersion/exposure intervals at each cross shore position at the monitoring section were identified at the wave run-up time series.
- The slope elevation along the measuring area was assumed to be the same respect to all the values taken from consecutive swash events.

3.5.3 Results and discussion

3.5.3.1 2D scanner performance

The wave run-up measurements taken from the 2D scanner were validated against the ultrasonic sensor measurements. Both at the time series, Figure 39, and at the scatter plots, the measurements from the ultrasonic sensors were characterized by pikes. The errors without waves were around $RMSE = 0.0043\text{ m}$ and $RMSE = 0.0089\text{ m}$ for the dry and submerged region of the slope, respectively. When waves were applied, the errors were found to be one order of magnitude higher respect to the previous case, with $RMSE = 0.0032\text{ m}$ ($x = 264.1\text{ m}$) and $RMSE = 0.017\text{ m}$ ($x = 269.8\text{ m}$). In general it was reported that the data from the ultrasonic sensors was underestimated by the 2D scanner, this occurred at all recording stations excepting $x = 267.9\text{ m}$, Fig. 4. The lower values can be attributed to the effect of the grazing angle and to the laser penetration inside the water, as station $x = 267.9\text{ m}$ was right above the scanner location. In general a good agreement between both approaches can be reported.

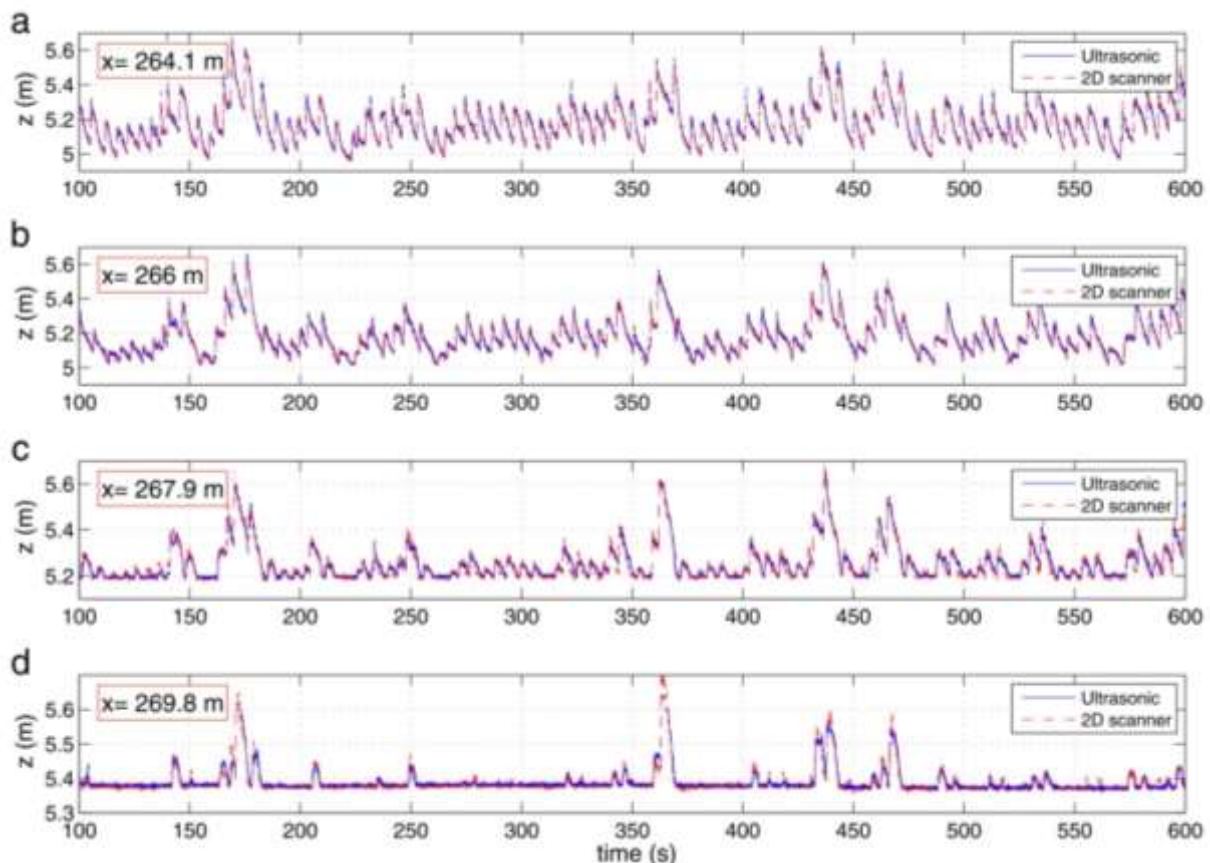


Figure 39: Wave run-up measured by the 2D scanner (red dashed lines) and ultrasonic sensors (solid blue line), at different stations. From (Vousdoukas, et al., 2014)

Nevertheless the satisfactory agreement between the 2D scanner and the ultrasonic sensors, some deviations of about 0.2 m can be reported at some locations, Fig. 4. The reported differences are due to the distance existing between the laser and ultrasonic monitoring sections. Also the horizontal area of the beam footprint (increasing as a

function of the grazing angle and the distance from the device) should be taken into account, as it affects the horizontal and vertical positioning accuracy. Besides, the performance of the 2D scanner can be affected by the grazing angle, for instance it can influence the laser beam point spacing, which is varying with the free surface elevation. Thus, when the measurements from the 2D scanner are compared to the ultrasonic sensors, this are considered as point measurements, but this is not correct as previous interpolation is necessary.

Another source of error is the refraction of the laser beam (according to Snell's law) when it penetrates the free surface. The refraction varies with the grazing angle, whereas the penetration depth is function of the turbidity and the water surface roughness. Furthermore, refraction plays a bigger role when measuring outside the swash zone, as due to the presence of foam and suspended material the water closer to the shoreline is characterized by higher reflectivity.

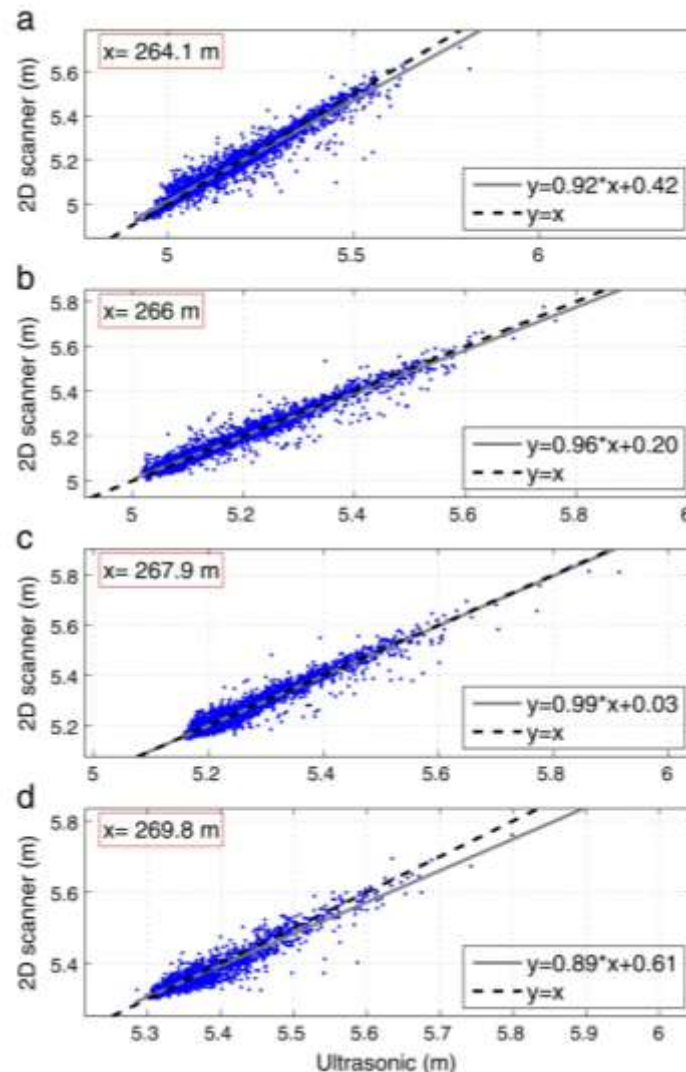


Figure 40: Scatter plots comparing the surface elevation measurements from the 2D scanner and the ultrasonic sensors, at different locations. Solid gray line shows the linear fit line (parameters shown in the legend), while the black dashed line expresses the perfect fit. From (Vousdoukas, et al., 2014)

3.5.3.2 Combination of laser scanner and video, benefits and capabilities

The developed technique is based on processing software which is part of the Orasis video monitoring system, with *ad hoc* routines for the laser scanner data. The major part of the software is open access.

The processing of the 2D laser scanner data is simplified by the colour information gathered from the video imagery. The information from the timestack images allows an easier interpretation of the swash events, i.e. dry and wet parts of the monitoring area. The imagery gathers data that is not available within the 2D scanner measurements. For instance, the foam following the backwash events can be confused with the slope surface when measuring with 2D scanner or ultrasonic sensors. But when analysing the timestack images the identification of foam is easy as it produces a high colour contrast with the slope and this errors are eliminated throughout the fusion of 2D laser scanner and video.

One of the most important uncertainty factors is the geo-rectification errors. But with the present technique by implementing the elevation measurements from the 2D laser scanner, the geo-rectification errors are minimized and the data from the video imagery is more reliable. Therefore it is demonstrated that the combination of video and laser scanner techniques improves the precision of video system applications, such as the case of monitoring wave run-up at the swash zone.

4 CONCLUSIONS

In this report, some recent developments concerning techniques for non-intrusive measurement of ocean waves were presented.

Sensors and techniques used for wave field measurement at sea were first presented. In this case, the non-intrusive instruments are placed above water, they present some major advantages compared to in-situ instruments. They are less subject to the marine environment and associated issues of wave loading, bio-fouling or corrosion for example. They can also be situated in very remote locations, for example in the case of airborne or spaceborne systems, which hugely limits the possibility of destruction by human activities.

Currently, space-borne synthetic aperture radar (SAR) is the only instrument providing directional ocean wave information on a global scale. Along and across track interferometric SAR measurements of ocean waves and currents were developed to measure simultaneously radar cross section, sea surface elevation and orbital velocity. The airborne InSAR systems flown so far are mainly used for scientific studies. However, the technique has reached a status where spaceborne missions for operational use are in the planning stage (COST, 2014). Such information is vital for the improvement of numerical models of global ocean dynamics, primarily used in the MRE industry for resource assessment and environmental impact studies.

Standard nautical X-band radar systems allow covering large measurement areas in short periods of time from a fixed location, on a platform or land-based. They are then suited to the survey of MRE field test sites. WAMOS II marine radars are in use at the EMEC test site to estimate the wave resource at two different berths. The comparisons of their measurements with those from Datawell Waverider MKIII buoys showed good agreement on significant wave height, peak period and peak wave direction. Agreement was not as good when compared to data from an ADCP, probably because of local effects on the ADCP measurements.

A WERA HF radar, specifically configured for wave field measurement, is in use at the Wave Hub test site for resource characterisation and environmental monitoring. This system, calibrated using data from a SeaWatch Mini II directional buoy, surveys an area measuring 75-by-90 km with 1 km spacing. Comparisons of radar measurements with in-situ point measurements obtained from an ADCP or a buoy here again presented some discrepancies, which can again be attributed to the fact that radar measurements are averaged over a large area while buoy and ADCP return local measurements. Comparisons of radar measurements with numerical simulations of the full site using the Wave-Watch III wave model of the site showed good correlation.

Arrays of remote-sensing instruments returning point-measurements have been used to measure the directional properties of ocean waves over smaller areas. Systems based on arrays of laser altimeters or ultrasonic transducers have been used with success to measure the directional properties of waves propagating over a small area, typically of tens of meters in width.

Another non-intrusive wave field measurement technique that presents an interest for MRE sites is stereo-photogrammetry. With this technique, a relatively restrained area of the ocean's surface is investigated to obtain the directional characteristics of the wave field. This technique is now mature for wave field measurement. Further developments in this technique include improving CCD cameras to obtain finer resolution and larger viewing areas obtain real-time estimation of the omnidirectional spectrum over the investigated area.

Lidars and flash lidars are very promising instruments for non-intrusive wave field measurement. Analysis techniques already have been developed for the analysis of flash lidar measurements of ocean waves that could lead to short-term forecasting of the ocean surface over a wide area. The technology is however still in development at the time of writing.

Wave field measurement is classically performed in wave tanks using resistive or capacitive wave probes. Non-intrusive instruments present different advantages over intrusive ones for experimental tests in wave tanks. The fact that they do not interfere with the wave field to be measured can be seen as their main advantage. This is indeed very useful when studying very small amplitude waves, like capillary waves. For such studies of small waves, optical systems have been developed. A system measuring the 2D-slope of the water surface using the reflection of a laser

beam was developed by Sanker and Shemer (Sanker & Shemer, 2012). Good results were obtained for slopes up to 44 degrees, and with high-frequency waves. Another system developed by Rabaud et al. uses the refraction of a pattern of dots through a glass walled water tank. They obtained good results in a 60 cm × 40 cm tank with few cm of water.

The disturbances of the wave field due to intrusive instrumentation, mostly due to radiated waves, become less important with the scale of the waves considered increasing. Studies concerned with the interaction of waves and structures, for example of wave energy converters, are usually carried out at scales varying between 1/100 and 1/5, with physically simulated waves of the order of few centimeters to few meters. The effects of waves radiated by resistive or capacitive wave gauges in the system can most often be considered negligible in such cases. Advantages of non intrusive instrumentation would be different for such studies, but still considerable.

Ultrasonic probes are now widely used in wave tanks. They allow good data rates and are easy to handle and install. They present the interest to only need as input their height above water to be calibrated, therefore returning more accurate measurements by minimising uncertainties due to calibration. However, some of their key performance parameters such as spot size and data rate vary with beam angle and working distance. The finite size of the acoustic beam can affect their measurements, as they can return data revealing a spatial averaging, for example at wave peaks and troughs. Their signal also drops out for steep waves. Finally they are not suitable for densely populated point measurements.

A surface elevation point measurement technique based on optical triangulation was developed at the University of Edimburgh, in which images from a camera looking at a laser pointing at the water surface are analysed. This system was shown to give better estimates of wave height than resistive wave probes, with comparative measurements matching more closely results from the fifth order Stokes theory. The system is suitable for small tank tests but, equipped with a moving assembly activated by a linear actuator for calibration, it is still rarely used.

Intrusive wave probes can also be a problem in a towing tank, when the wave created by a wave probe moving with the carriage, and its loading, become non-negligible. Non-intrusive wave elevation measurement can for such cases be an advantage, and acoustic probes are more and more used. Optical techniques can also be used, like the laser-sheet technique developed by Perelman et al. (Perelman, Wu, Boucheron, & Fréchet, 2011). Its setup is not easy however.

Some non-intrusive instruments also present the advantage of carrying out instantaneous multi-dimensional measurements, i.e. 1D-wave elevation measurements on a line, or 2D-wave field measurements over an area. Such instruments are able to replace wave probe arrays, which can be difficult to install and interfering with the body/bodies studied.

Scanning lidars, which recently made their way to coastal engineering labs, are an example of instrumentation returning 1D-wave measurements. Blenkinsopp et al. obtained good agreement between lidar and capacitance wave probes. They still noticed problems of laser return with clear water, linked to the beam's incidence angle on the water surface. They obtained better results by adding some clay to the water to obtain specular reflections. The same kind of lidar was also used by Vousedoukas et al., (2014) at the FZK of Leibniz Universität Hannover (LUH) in a study of wave dynamics at the swash zone combining data from several non-intrusive instruments. The system they developed uses three cameras, height ultrasonic gauges and a scanning lidar, and can provide continuous measurement of the free surface elevation at the swash zone in 2D-space and time.

Stereo-imaging has shown to provide reliable wave elevation measurements at sea, but it is a very challenging technique to implement in wave tanks. Different strategies have been tested to overcome poor matching results, like spraying the free surface with a mist, or seeding with floating particles. None seems yet to have been developed that could be easily implemented in most coastal engineering laboratories, and research in this domain is still needed. The potential application of this technique in a carefully controlled environment like a wave tank would be very valuable for experimental studies, engineering design and validation of numerical codes.

5 REFERENCES

- ACT, A. f. (2012). *Waves measurement systems test and evaluation protocols*.
- Barrick, D. (1972). *Remote Sensing of the Troposphere- Ch. 12: Remote sensing of the sea state by radar*. V. E. Derr Ed.
- Barrick, D. (1977). Extraction of wave parameters from measured HF radar sea-echo Doppler spectra. *Radio Sci.* (12), 415-424.
- Barrick, D., & Weber, B. (1977). On the non-linear theory for gravity waves on the ocean's surface. Part II: Interpretation and applications. *Journal of Physical Oceanography* (7), 11-21.
- Bechle, A., & Wu, C. (2011). Virtual wave gauges based upon stereo imaging for measuring surface wave characteristics. *Coastal Engineering* (58), 305-316.
- Benetazzo, A. (2006). *Measurement of water surface wave fields using a non-intrusive method based on a stereo-matching algorithm*. PhD thesis, University of Padua.
- Benetazzo, A. (2006). Measurements of short water waves using stereo matched image sequences. *Coastal Engineering* (53), 1013-1032.
- Birch, R., Fissel, D., Borg, K., Lee, V., & English, D. (2004). The Capabilities of Doppler Current Profilers for Directional Wave Measurements in Coastal and Nearshore Waters. *Oceans '04 MTS/IEEE*. Kobe, Japan.
- Blenkinsopp, C., Turner, I., Allis, M., Peirson, W., & Garden, L. (2012). Application of LiDAR technology for measurement of time-varying free-surface profiles in a laboratory wave flume. *Coastal Engineering* (68), 1-5.
- Boudière, E., Maisondieu, C., Ardhuin, F., Accensi, M., Pineau-Guillou, L., & Lepasqueu, J. (2013). A suitable metocean hindcast database for the design of Marine energy converters. *International Journal of Marine Energy*, 40-52.
- Challenor, P. W. (2008). Satellite altimetry: A revolution in understanding the wave climate. *Proceedings of the Symposium on 15 Years of Progress in Radar Altimetry*, (pp. 13-18). Venice, Italy.
- Christensen, K., Röhrs, J., Ward, B., Fer, I., Broström, G., Saetra, Ø., & Brevik, Ø. (2013). Surface wave measurements using a ship-mounted ultrasonic altimeter. *Methods in Oceanography* (6), 1-45.
- COST Action714. (2005). *Measuring and analysing the directional spectra of ocean waves*.
- Essen, H., Gurgel, K., & Schlick, T. (1999). Measurement of ocean wave height and direction by means of HF radar: An empirical approach. *Dt. hydrogr. Z.* (51), 369-383.
- Fedele, F., Benetazzo, A., Gallego, G., Shih, P., Yezzi, A., Barbariol, F., & Ardhuin, F. (2013). Space-time measurements of oceanic sea states. *Ocean Modelling* (70), 103-115.
- Fernandez, D., Graber, H., Paduan, J., & Barrick, D. (1997). Mapping wind direction with HF radar. *Oceanography* (10), 93-95.
- Gallego, G., Yezzi, A., Fedele, F., & Benetazzo, A. (2011). A Variational Stereo Method for the three-dimensional reconstruction of ocean waves. *IEEE Trans. Geosci. Remote Sens.* (vol.49, no.11), 4445-4457.
- Good, A., Hamill, G., Whittaker, T., & Robinson, D. (2011). PIV Analysis of the Near Wake of a Tidal Turbine. *Proceedings of the Twenty-first (2011) International Offshore and Polar Engineering Conference*. Maui, Hawaii, USA.
- Grilli, S., Guerin, C., & Goldstein, B. (2011). Ocean Wave Reconstruction Algorithms Based on Spatio-temporal Data Acquired by a Flash LIDAR Camera. *Proceedings of the Twenty-first International Offshore and Polar Engineering Conference*. Maui, Hawaii, USA.
- Gurgel, K., Antonischki, G., Essen, H., & Schlick, T. (1999). Wellen Radar (WERA), a new ground-wave based radar for ocean remote sensing. *Coastal Eng.* (37), 219-234.
- Gurgel, K., Antonischki, G., Essen, H., & Schlick, T. (1999). Wellen Radar (WERA): a new ground-wave HF radar for ocean remote sensing. *Coastal Engineering* (37), 219-234.
- Gurgel, K., Essen, H., & Kingsley, S. (1999). High-frequency radars: physical limitations and recent developments. *Coastal Eng.* (37), 201-218.
- Gurgel, K., Essen, H., & Schlick, T. (2006). An empirical algorithm to derive ocean waves from second-order Bragg scattering: prospects and limitations. *IEEE Journal of Oceanic Engineering* (V.31, no.4).
- Hashimoto, N., & Tokuda, M. (1999). A Bayesian approach for estimation of directional wave spectra with HF radar. *Coast. Eng. Journal* (V. 41).

- Haus, B., Ramos, R., Graber, H., Shay, L., & Hallock, Z. (2006). Remote observation of the spatial variability of surface waves interacting with an estuarine outflow. . *IEEE Journal of Oceanic Eng.*, 31(4), 835-849.
- Haus, B., Shay, L., Work, P., Voulgaris, G., Ramos, R., & Martinez-Pedraja, J. (2010). Wind speed dependence of single-site wave-height retrievals from high-frequency radars. *Journal of Atmospheric and Oceanic Technology*, 27, 1381-1394.
- Heron, S., & Heron, M. (1998). A comparison of algorithms for extracting significant wave height from HF radar ocean backscatter spectra. *Journal of Atmospheric and Oceanic Technology*, 15, 1157-1163.
- Hisaki, Y. (1996). Nonlinear inversion of the integral equation to estimate ocean wave spectra from HF radar. *Radio Sciences*, 31(1), 25-39.
- Hofland, B., Hoffmann, R., & Lindenbergh, R. (2012). Wave measurement techniques for the new large-scale delat flume. *Proc. Coastlab*. Gent, Belgium.
- Holthuijsen, L. (2007). *Waves in oceanic and coastal waters*. Cambridge.
- Howell, R., & Walsh, J. (1993). Measurement of ocean wave spectra using narrow beam HF radar. *Radio Sciences*, 18(3), 296-305.
- Hwang, P., Wang, D., Walsh, E., Krabill, W., & Swift, R. (2000). Airborne Measurements of the Wavenumber Spectra of Ocean Surface Waves. Part I: Spectral Slope and Dimensionless Spectral Coefficient. *J. Physical Oceanography (V.30)*, 2753-2767.
- IEA-OES. (2009). Wave data catalogue for resource assessment in IEA-OES member countries. *Implementing Agreement on Ocean Energy Systems*.
- Irish, J., Wozencraft, J. C., & Giroud, C. (2006). Nonintrusive Measurement of Ocean Waves: Lidar Wave Gauge. *Journal of Atmospheric and Oceanic Technology* 23 (11), 1559-1572.
- Jackson, C., & Apel, J. (2004). *Synthetic Aperture Radar Marine User's Manual*. Washington, D.C.: U.S department of commerce.
- Jähne, B. (1993). *Spatio-Temporal Image Processing — Theory and Scientific Applications*. Berlin Heidelberg: Springer-Verlag.
- Kahma, K., Hauser, D., Krogstad, H., Lehner, S., Monbaliu, J., & Wyatt, L. (2005). *Measuring and analysing the directional spectra of of ocean waves*. EU COS Action 714, EUR 21367.
- Krogstad, H., Barstow, S., Mathisen, J., Lønseth, L., Magnusson, A., & Donelan, M. (2008). Extreme Waves in the Long-Term Wave measurements at Ekofisk. *Proc. Rogue Waves Workshop*, (pp. 23–33). Brest, France.
- L.R., W. (1988). Significant waveheight measurement with HF radar. *International Journal of Remote Sensing*, 9, 1087-1095.
- L.R., W. (1990). A relaxation method for integral inversion applied to HF radar measurement of the ocean wave directional spectrum. *International Journal of Remote Sensing*, 11, 1481-1494.
- Liberzon, A., Gurka, R., & Hetsroni, G. (2004). XPIV - Multi-plane Stereoscopic Particle Image Velocimetry. *Experiments in Fluids*, 36(2), 355-362.
- Lipa, B. (1977). Derivation of directional ocean-wave spectra by integral inversion of second-order radar echoes. *Radio Sciences*, 12, 425-434.
- Liu, H., Katsaros, K., & Weissman, M. (1982). Dynamic response of thin-wire gauges. *Journal of geophysical research* (87), 5686–5698.
- Lopez, G., Conley, D., Magagna, D., & Greaves, D. (2013). Adjusting An Empirical Algorithm for Extracting Wave Height from HF Radar Measurements at the Wave Hub. *EWTEC 2014*. Aalborg, Denmark .
- Luther, M., Meadows, G., Buckley, E., Gilbert, S., Purcell, H., & Tamburri, M. (2013). Verification of Wave Measurement Systems. *Marine Technology Society Journal*, V.47, n.5.
- Maresca, J., & and Georges, T. (1980). Measuring rms wave spectra using narrow-beam HF radar. *IEEE J. Oceanic Eng.*, 18, 295-305.
- Martin, S. (2014). *An Introduction to Ocean Remote Sensing*. Cambridge Univ. Press.
- Osterried, M. H. (2010). *Power from waves: Oscillating Wave Surge Converters in the near-shore region*. Belfast: PhD thesis, QUB.
- Payne, G., Richon, J., Ingram, D., & Spinneken, J. (2009). Development and preliminary assessment of an optical wave gauge. *Proceedings of the 8th European Wave and Tidal Conference*, (pp. 160-167). Uppsala, Sweden.
- Perelman, O., Wu, C., Boucheron, R., & Fréchet, D. (2011). 3D wave field measurement techniques in model basin: Application to ship wave measurement. *Advanced Model Measurement Technology for EU Maritime Industry*.

- Piepmeyer, J., & Waters, J. (2004). Analysis of Stereo Vision-Based Measurements of Laboratory Water Waves. *IEEE International Geoscience and Remote Sensing Symposium Proceedings: Science for Society: Exploring and Managing a Changing Planet*, 3588-3591.
- Pitt, E. (2005). Estimating Power from Wave Measurement at the European Marine Energy Centre (EMEC) Test Site.
- Pitt, E. (2005). *Estimating power from wave measurements at the European Marine Energy Center (EMEC) test site*. AWR.
- Ramos, R., Graber, H., & Haus, B. (2009). Observation of wave energy evolution in coastal areas using HF radar. *J. Atmos. Oceanic Technol.*, 26, 1981-1909.
- Robinson, I. (2004). *Measuring the Oceans from Space: The Principles and Methods of Satellite Oceanography*. Springer Science & Business Media.
- Ross, D., Peloquin, R., & Sheil, R. (1968). Observing ocean surface waves with a Helium neon laser. *Proc. 5th Symp. on Military Oceanography*. Panama City.
- Sanker, E., & Shemer, L. (2012). Laser Slope Gauge for measuring 2D wave slopes. *32nd Israeli Conference on mechanical engineering*. Tel-Aviv, Israel.
- She, K., & Cannings, P. (2007). Geometric study of monochromatic waves breaking on beaches. *Journal of Waterway, Port, Coastal, and Ocean Engineering*, 334-342.
- Stewart, R. (1985). *Methods of Satellite Oceanography*. University of California Press.
- Stewart, R. (2008). *Introduction To Physical Oceanography*.
- Sun, J., Burns, S., Vandemark, D., Donelan, M., Mahrt, L., Crawford, T., . . . French, J. (2005). Measurement of Directional Wave Spectra Using Aircraft Laser Altimeters. *Journal of Atmospheric and oceanic technology* (22), 869-885.
- Venugopal, V., Davey, T., Smith, H., Smith, G., Holmes, B., Barret, S., . . . Girard, F. (2011). D2.2.: Wave and Tidal Resource Characterisation. *EQUIMAR*.
- Victor, L., Troch, P., & Kofoed, J. (2011). On the Effects of Geometry Control on the Performance of Overtopping Wave Energy Converters. *Energies*, 4, 1574-1600.
- Vousdoukas, M., Kirupakaramoorthy, T., Oumeraci, H., de la Torre, M., Wübbold, F., Wagner, B., & Schimmels, S. (2014). The role of combined laser scanning and video techniques in monitoring wave-by-wave swash zone processes. *Coastal Engineering* (83), 150-165.
- Wanek, J., & Wu, C. (2006). Automated trinocular stereo imaging system for three-dimensional surface wave measurements. *Ocean Engineering* 33 (5-6), 723-747.
- Weber, B., & Barrick, D. (1977). On the nonlinear theory for gravity waves on the oceans's surface. Part I: Derivations. *Journal of Physical Oceanography* (V.7, no.7), 3-10.
- Wyatt, L. (1990). A relaxation method for integral inversion applied to HF radar measurement of the ocean wave directional spectrum. *International Journal of Remote Sensing*, 11, 1481-1494.
- Wyatt, L. (1997). The ocean wave directional spectrum. *Oceanography*, 10, 85-89.
- Wyatt, L. (2002). An evaluation of wave parameters measured using a single HF radar system. *Canadian Journal of Remote Sensing*, 28, 205-218.
- Wyatt, L. (2007). Wave and tidal power measurement using HF radar. *Proceedings of IEEE Oceans'07*. Aberdeen, UK.
- Wyatt, L., Venn, J., Moorhead, M., Burrows, G., Ponsford, A., & van Heteren, J. (1985). HF radar measurements of significant waveheight and mean period during NURWEC. *Advances in Underwater Technology and Offshore Engineering*, 4, 209-222.
- Zhang, J., Walsh, J., & Gill, E. (2012). Inherent limitations in high-frequency radar remote sensing based on Bragg scattering from the ocean surface. *IEEE Journal of Oceanic Engineering*, 37(3).